UNIVERSITY OF CALIFORNIA,
IRVINE

Dynamics of Chemi-Ion Driven Flows in an Applied Electric Field

THESIS

submitted in partial satisfaction of the requirements
for the degree of

MASTER OF SCIENCE

in Mechanical and Aerospace Engineering

by

Jesse A. Tinajero

Thesis Committee:
Professor Derek Dunn-Rankin, Chair
Professor Jack Brouwer
Professor Vincent McDonell

2015

DEDICATION

To my family.

TABLE OF CONTENTS

LIST OF FIGURES

LIST OF TABLES

ACKNOWLEDGMENTS

I would like to thank Professor Dunn-Rankin for granting me this opportunity to work on such an interesting research topic. Without his patience and guidance, this thesis would not be possible.

I would like to thank the other graduate students who have laid the ground work for this thesis. The two most notable are Sunny Karnani and Alice Chien. Their experience and wealth of knowledge provided me with both the necessary tools to build the experiments in this thesis and a pathway to interpreting the results.

I would also like to thank my lab mates for their encouragement and the intellectual conversations we have had throughout the course of my graduate studies. They continuously challenge me to think in new ways and push me to improve my skills and build upon my knowledge.

This work is supported by NASA ISS Research Project via agreement NNX11AP42A, with Dennis Stocker as contract monitor.

ABSTRACT OF THE THESIS

Dynamics of Chemi-Ion Driven Flows
in an Applied Electric Field

By

Jesse A. Tinajero

MASTER OF SCIENCE in Mechanical and Aerospace Engineering

University of California, Irvine, 2015

Professor Derek Dunn-Rankin, Chair

Chemi-ions are produced during combustion of a hydrocarbon fuel. If an external electric field is present, a charge separation occurs due to the electrical force acting on the positively and negatively charged species. These ions traverse in the direction of the electrode of opposite potential. Along their path, they continuously collide with neutral molecules within the surrounding bulk gas until they are able to recombine and neutralize at the downstream electrode. During each collision, the charged species give up their acquired momentum to the neutral molecules. Macroscopically, this transfer of momentum has been best described mathematically as a body force acting on the bulk gas. The effect is commonly referred to as an ion wind effect.

Gravity effects make the electric field effects on combustion difficult to study with earth-based experiments. This is because the gravity-driven buoyancy effects behave as a body force also acting on the bulk gas. Buoyancy and electrical body forces act on the same order of magnitude. The two forces are coupled through temperature since the production of ions is temperature dependent. Between the two, the contribution to the net momentum of the gas is then difficult to distinguish. On the other hand, micro-gravity experiments allow for the direct study of electric field effects in the absence of gravity. Micro-gravity experiments

on-board the International Space Station through NASA's Advanced Combustion via Microgravity Experiments program, or ACME, are planned for 2016-17. Nevertheless, preliminary studies are needed in preparation for the ISS experiments. These studies are described in this thesis.

A replica of the ISS experiment for the electric field effects on laminar diffusion flames (EFIELD Flames) that is part of ACME was recreated in a ground based laboratory. A schlieren system was built to visualize the effect an applied electric field has on the flame's buoyant thermal plume when the electric field is given a step function. Thermal plumes created by natural convection are well understood and can be related to parameters such as heat release and local velocity. Thus, when studying thermal plumes created by forced convection, i.e., ion wind effects, it is thought that similar relations can be made with electrohydrodynamic parameters such as ion current and electric potential.

High-speed videos captured the disturbance in the bulk gas due to a sudden presence of an applied electric field. These videos reveal a never before seen wave phenomenon that is created as the bulk gas transitions from a buoyancy driven gas flow to an electrically driven gas flow. Total ion current measurements were taken by using a shunt resistor in series with the high voltage power supply and the two electrodes. The experiments performed were focused on transient effects in order to characterize time-scales related to generation of both an ion current and ion wind. It was seen that the generation of an ion current was fully established within ≈10ms. This time-scale, however, may have been inhibited by a characteristically slow high voltage power supply system. The first noticeable appearance of an ion wind effect being generated was also seen to be ≈10ms. The time-scale related to a volume of "ion wind driven" gas cloud to travel the length of the electrode space region was seen to be ≈40ms for a 3.5cm electrode space length. The time-scale related to the time it takes for the bulk gas to reach a new steady state was seen to be ≈100ms. Finally, it was also observed that the time-scale related to the disappearance of visible soot when the

flame was compressed by an ion wind was ≈300ms. These experimental time-scales were then compared to time-scales developed through simplified electrical aspects of combustion theory. Both theoretical and experimental time-scales appeared to agree within reason.

Chapter 1

Introduction

The observed effects on combustion with an applied electric field have been best described by an ion wind effect (also known as Chattook wind). This ion wind effect has been described in the literature as the mechanical drag on the mostly neutral gaseous medium due to a flux of charged particles. Mathematically, it has been described as a body force, F_e, in the momentum equation. When described in this way, the electrical body force is analogous to the buoyancy force which occurs because of gravity and the presence of density variations within the gas. In fact, Papac [28] used an electric field to cancel the effects of gravity on an inverted capillary jet flame in a ground-based laboratory. While the effects of gravity were not completely canceled, the paper served well as a proof of concept and showed the importance of studying electric field flame dynamics (EFFD) in a micro-gravity environment. That is, no matter what geometry of the combustion system, buoyancy is always going to cloud the observed effects in earth-based EFFD studies. Thus, the optimum place to truly isolate the electric field effects from buoyancy is to perform the desired experiments in a micro-gravity based laboratory.

The study of EFFD in micro-gravity is not a new concept. Carleton and Weinberg published

an article in 1987 describing a proof of concept for a hand held, battery powered device that used small electric fields to control and direct convection in absence of gravity [5]. In 2006, Dunn-Rankin and Weinberg published a review which compiled various studies from both research groups dealing on the topic of EFFD [6]. More recently, Karnani performed 2.1 second drop tower experiments and showed the effect of an electric field on a micro-gravity flame [19]. This study showed the inverse of Papac's study where an electric field was used to simulate buoyancy effects on the micro-gravity flame.

The use of electric fields to assist combustion has many potential applications; both terrestrial and extraterrestrial. Weinberg studied the possibility of using an electric field as a sensing mechanism to warn when a quenching plate is in close enough proximity for the release of CO [40]. This has an obvious practical importance for harmful emissions inside combustion chambers in power generation systems. In 1966, Place published a paper describing the effects an applied electric field has on flame carbon [31]. A few years later, Mayo did a more in depth study of these effects [26]. These two studies describe the practicality of using external electric fields to control soot. Miller et al. stated the potential for using electric fields to suppress acoustic instabilities in jet engines [27].

Using relatively high electric fields (less than those that will produce electrical breakdown in the gaseous medium) to actively control a flame has been one of the primary motivations for studying EFFD for as long as the topic has been around. Borgatelli [1] studied the possibility of electric field control by demonstrating that the flame is not just the system intended to be controlled but also an active component of the electrical circuit as well. This concept is not only crucial for active control, but for sensing as well.

The motivation for studying EFFD has been shown consistently throughout the literature and restated in this introduction. As stated earlier, the importance of studying EFFD in micro-gravity is absolutely crucial to understanding many of the observed effects and the limits to which electric fields can be used for practical purposes. The intention of this thesis

is to perform the necessary experiments needed in order to prepare for such micro-gravity experiments. This thesis will do so by performing ground-based experiments on a laminar, diffusion methane flame in the presence of an applied electric field. The goal for these experiments is to study the dynamics of several phenomena;

- Production of an ion current due to a sudden presence of an applied electric field
- Disturbance of flow field due to the presence of the ion current
- Alterations to combustion parameters due to electro-hydrodynamics changing with time
- Measuring important time-scales related to these changes
- Comparing these measured time-scales to time-scales computed from theory

Chapter 2

Literature Background

The presence of ions in hydrocarbon flames has been demonstrated as far back as the 16th century. Research in the electrical properties of flames picked up speed in the 1940's and reached it's peak in the 1960's and 70's. Numerous studies have been performed to answer the questions of how/where ions are formed, what role do they play in combustion, and what advantages can they provide for practical purposes?

The purpose of this chapter is to provide a brief review of the literature related to the fundamental understanding of the work in the following chapters. The theory presented here is also necessary for the interpretation and analysis of the results of the experiments. Several historical reviews are referred to for a more detailed understanding, e.g. [36, 23, 27, 7, 10, 32]. This chapter will highlight the major points from these historical papers, as well as many others.

Section 2.1, will provide an explanation of the mechanisms involved in ion chemistry within a flame. The steps in the ion chemistry process include the initial ion-formation mechanisms, ion chain-branching mechanisms, and finally recombination. This section will proceed to identify the dominant charged species that have been determined to be present in and near a

flame. CHO^+ has been determined to be the kick-starter of the ion-chain processes. H_3O^+ has been determined to be the ion of most significance due to its high concentrations and long-life spans, e.g. [32].

Section 2.2, explains the ion motion induced by an electric field and its interaction with the surrounding bulk gas. The description of this interaction will assist in describing the generation of an ion wind. This section is particularly important for the fundamental understanding of Chapter 3.

Ultimately, the generation of an ion wind has been thought to be the source of the observable effects on combustion. The opposing argument is based on chemical effects. While chemical effects cannot be completely discredited, the ion wind effect appears to provide the best explanation for the observed phenomena. This will be described in Section 2.2.2 and will conclude the literature review in this chapter.

2.1 Ion Chemistry

Electrical aspects of combustion could most generally be split into two categories; flame ionization and electric field flame dynamics. This thesis focuses mostly on the latter. However, the electric field effects on flames cannot be studied without at least a basic understanding of flame ionization. Flame ionization deals with ion chemistry and has proven to be a very challenging topic for researchers to this day due to the complexity of the combustion process and the need for more accurate techniques for measuring short-lived ions. The importance of a better understanding of flame ionization, as well as, a need for a reduced ion chemistry mechanism is stated here but is not the focus of this thesis. The literature on flame ionization is seemingly endless, therefore, this section will provide a summary of the important points needed for a fundamental understanding in upcoming chapters.

The overall chain of events that leads to the production and destruction of ions in hydrocarbon flames can be broken down into three basic, sequential steps; initial formation, charge rearrangement, and recombination. Sudgen summarized each of these three steps by a single process [12, 36],

$$CH + O \rightarrow CHO^{+} + e^{-}, \tag{2.1a}$$

$$CHO^{+} + H_2O \rightarrow CO + H_3O^{+}, \tag{2.1b}$$

$$e^{-} + H_3O^{+} \rightarrow H_2O + H, \tag{2.1c}$$

where Equations (2.1a), (2.1b), & (2.1c) represent each of the three sequential steps, respectively.

The overall ion chemistry for a premixed methane-oxygen flame was detailed experimentally by Goodings, [10, 11], using a mass spectrometer. More recently, Prager's ion chemistry model, [32], showed to be in agreement with Goodings data; the most notable discrepancy being the ion CHO^{+}.

2.1.1 Initial Ion Formation Processes

Chemi-ionization has been accepted as the important ion formation mechanism in hydrocarbon flames; the product of chemi-ionization being CHO^{+}. Other mechanisms that have been presented in competition with chemi-ionization include (Lawton et al. [25]),

- Ionization by collision
- Electron transfer & Hot Electron Collision
- Ionization by transfer of excitation energy
- Thermionization of particles

Chemi-Ionization

Chemi-ionization is defined as,

$$A + B \rightarrow C^+ + D + e^-, \tag{2.2a}$$

$$A + B \rightarrow C^+ + D^-. \tag{2.2b}$$

Both Equations (2.2a) and (2.2b) are unique from other ion formation processes by the fact that two neutral molecules go through a process of chemical rearrangement leading to product species with both a positive and negative charge.

It can be easily seen that Equation (2.1a) fits this description. Determination of Equation (2.1a) being the significant ion formation mechanism can be found in countless historical papers, e.g. [3, 7, 12].

Ionization by Collision

Ionization by collision can occur in two ways; collision between two neutral molecules or collision between a neutral molecule and electron.

$$A + B \rightarrow A^+ + B + e^- \tag{2.3a}$$

$$A + e^- \rightarrow A^+ + e^- + e^- \tag{2.3b}$$

The major difference between ionization by collision and chemi-ionization is that the reactants maintain their chemical composition but have lost an electron.

The maximum conversion of kinetic energy to internal energy, U_{max}, during the collision of

two particles is given by the equation

$$U_{max} = \frac{1}{2}\frac{M_1 M_2}{(M_1 + M_2)} v_r^2, \tag{2.4}$$

where v_r^2 is the intial relative velocity of the two particles, M is the mass of the particle, the subscripts 1 and 2 represent particles 1 and 2, respectively. If Equation (2.4) is taken from the frame of reference of particle 2 then the maximum conversion to internal energy is expected to occur when $M_1 \ll M_2$, as in the case of an electron colliding into a molecule. It was concluded (Fialkov et al. [7]) that the ion concentration produced by collision are many orders of magnitude less than are actually present in flames.

Electron Transfer & Hot Electron Collision

Ionization due to electron transfer is simply defined by a collision of two initially neutral molecules resulting in a transfer of an electron from one to the other.

$$A + B \rightarrow A^+ + B^- \tag{2.5}$$

Since ionization potentials tend to be higher than electron attachment energies. Therefore, electron transfer reactions tend to be endothermic.

Ionization through hot electron collision, on the other hand, is the process involving a collision of a free electron elevated to high electron temperatures ($\approx 3\times10^4 K$) with a neutral molecule. The result is an electron is released from the molecule as seen below,

$$A + e^- \rightarrow A^+ + 2e^-. \tag{2.6}$$

While ionization of this type has been seen in flames, it has been accepted to not be of significance, [7].

Ionization by Transfer of Excitation Energy

Molecules elevated to an excitation state are present in flames and have sufficiently long enough lifetimes to participate in many collisions. Thus, ionization of this type have been suggested to participate in flame ion production. The process transfer of excitation energy from the excited molecule to another molecule. This transfer of energy is significant enough to release an electron. The form of the this process is described as,

$$A^* + B \rightarrow A + B^+ + e^-. \tag{2.7}$$

A reaction of this type has been proposed for fuel-rich flames.

$$CH^* + C_2H_2 \rightarrow {C_3H_3}^+ + e^- \tag{2.8}$$

Equation (2.8) is thought to be the source of ${C_3H_3}^+$ which has been seen to be in high concentrations in fuel-rich flames.

2.1.2 Charge Rearrangement

Section 2.1.1 discussed the possible processes involved with the initial formation of flames ions. It was stated that chemi-ionization is the dominant ion formation mechanism with CHO^+ as the parent chemi-ion. However, its well known that other ions, such as H_3O^+ and ${CH_3}^+$ are present in flames, e.g. [25]. In fact, Many of these ions have been seen with much higher concentrations and further from the flame than CHO^+. This section is dedicated to the reactions involving ion-molecule interactions and electron attachment resulting in the production of new flame ions.

Proton Exchange

The reaction from Equation 2.1b is an example of a proton exchange process. These types of reactions have been seen to be very in important in the production cycle of flame ions. More generally it described as,

$$AH^+ + B \rightarrow A + BH^+. \tag{2.9}$$

The majority of flame ions (with the except of the obvious CHO^+ ion) are thought to be produced through proton exchange.

Electron Transfer

A transfer of an electron can occur between a molecule and an ion such as,

$$A + B^+ \rightarrow A^+ + B. \tag{2.10}$$

If B is the ion form of A, then $\triangle H = 0$. If the A and B are dissimilar then $\triangle H \neq 0$ and the collisional cross-sections are most likely small.

Dissociative Attachment

Dissociative attachment is a form of electron attachment. An example of this is describes by,

$$A_2 + e^- \rightarrow A + A^-. \tag{2.11}$$

For this reaction to occur, the minimum energy the electron must posses is the difference between the dissociative energy and the electron affinity of the attaching species ($V_d - V_a$).

Radiative Attachment

Radiative attachment has been known to occur in flames but is relatively slow. Thus, it is not considered an important pathway for charge rearrangement. These reactions are of the form

$$A + e^- \rightarrow A^- + h\nu. \tag{2.12}$$

Three-Body Attachment

Three body attachment can most generally be described as,

$$A + e^- + X \rightarrow A^- + X. \tag{2.13}$$

The third body, denoted as X, is needed to absorb excess energy. Reactions of this type are more likely at high pressures due the probability of a collision between the three species.

2.1.3 Recombination

The third and final step is the neutralization of charges. For this to occur, both positive and negative charges must be present in the same region.

Three-Body Recombination

During a three-body recombination reaction, energy is released during the collision of a positive/negative ion pair. A third body is needed for this reaction in order to dissipate the energy of the recombination.

$$A^+ + e^- + X \rightarrow A + X \tag{2.14a}$$

$$A^+ + B^- + X \rightarrow A + B + X \tag{2.14b}$$

Dissociative Recombination

During a collision between an electron and a charged molecule, the electron can attach itself to the molecule. This recombination forces the molecule to dissociate. This is described as,

$$AB^+ + e^- \rightarrow A + B. \tag{2.15}$$

Mutual Neutralization

Mutual Neutralization occurs during the collision between two oppositely charged ions. The charge is transferred and the excess energy leaves the neutral molecules in an excited state.

$$A^+ + B^- \rightarrow A^* + B^* \tag{2.16}$$

2.1.4 Ion Chemistry Final Remarks

Research on the ion chemistry in flames is a very extensive topic. This section has touched only a small portion of an endless supply of ion chemistry studies. The conclusions of these

studies have shown that Equations (2.1a)-(2.1c) could most simply describe the full process of ionization. Mass spectroscopy studies (e.g. [10]) have detailed the important charged species in hydrocarbon flames. The most notable ions being CHO^+ as the parent ion, H_3O^+ as the positive ion of highest concentration, and electrons as the most important negatively charged species. However, the reality is ion chemistry is much more complex. This can be seen in the study on the ion formation kinetics in a methane air flame produced by Starik and Titova [35] in 2002. The authors used 214 ion reactions and 20 ions species, including negative ions and nitrogen containing ions. In a study on electric field effects on premixed methane flames performed by Pederson and Brown in 1993 [30], the authors used a much simpler ion chemistry model containing 86 ion reactions. The authors found the model to produce a peak ion current saturation close to stoichiometry. However, the model was found to predict ion species profiles less accurately for fuel-rich flames when compared to experimental data. One of the more recent detailed ion chemistry model used in simulations [32] was discussed earlier in this chapter. Prager's lean methane-oxygen model consisted of 67 ionic reactions and produced good aggreement to experiments.

It has been shown in these studies, as well as others, that other ions must be considered important when moving from the fuel-lean to fuel-rich regimes; CH_3^+ and $C_3H_3^+$ being two ions that have been measured in high concentrations in sooting flames. $C_3H_3^+$ is considered to be another parent ion that is produced independently from CHO^+ in fuel-rich flames, [25] et al. Vinckier et al. showed $C_2H_3O^+$ is considered a secondary parent ion after CHO^+ [37]. The ionization mechanisms due to additives or small particles are not discussed in this thesis. Instead, an interested reader is referred to by Fialkov's review [7].

2.2 Ion-Driven Flows

It has been well documented since the 1800's that applied electric fields produce dramatic effects on combustion. Extension of blow-off limits, reducing flame carbon, stabilizing flames, increasing flame velocity, and increasing luminosity are some of the observed effects seen throughout the literature. It is clear that these effects are a result of molecular collisions between charged species and neutral molecules. The question is then, "What types of collisions dominate; elastic or nonelastic"? Within the electric aspects of combustion community, the debate has broken down into two arguments; a fluid-mechanical effect (ion wind) vs chemical effects.

One example from the literature favoring chemical effects was from Jaggers and Engel [16]. In this research, the authors measured an increase in laminar flame speed under the influence of high AC fields. They concluded that their applied AC field had a high enough frequency to produce an increase in electron energy while the translational effects on positively charged ions must have been negligible due to their lower mobilities. Thus, the energized electrons must have been the source of the observed increase in burning velocities. Furthermore, since electrons do not create a large mechanical drag effect (high mobility) the electron/neutral collisions must be opening new chemical pathways. Bowser and Weinberg [2] challenged this by stating that a burner stabilized flat flame is a much more reliable method for measuring burning velocities since small mechanical drag could alter the flame area when experimenting with propagating flames. These authors then showed no change in burning velocity when a field was directed such that a flux of electrons was directed through the reaction zone. Thus, these results provided stronger evidence that an ion wind effect is the cause of observed effects rather than chemical effects.

The previous chapter dealt with the chemistry aspects of ions in flames. The goal of ion chemistry is to discover the important ion species and reaction mechanisms, as well as, mea-

sure parameters such as rate constants and enthalpy of formation. This section attempts to connect the molecular aspects of flame ionization to the observed effects on the macroscopic level. That is, how do these ion species behave when an externally generated electric field is present? How do these charged species travel through a neutral gaseous medium? What effects do they create in the carrier gas medium? This will be done through an ion wind explanation (elastic collisions).

2.2.1 Ion Wind

A charged particle that is accelerated by an electric field in a vacuum is given no resistance to accelerate. Thus, the kinetic energy given to the molecule is equal to the change in potential energy. Since the potential energy is governed by the electric potential, the velocity of the particle is described by,

$$v = \sqrt{\frac{2q \triangle V}{m}}. \tag{2.17}$$

Here, q is the charge of the particle, $\triangle V$ is the difference in electric potential from state 1 to state 2, and m is the mass of the particle.

However, this study is interested in the effects of many charged particles in a mostly neutral gas medium. From now on the term species will be used in replacement of the term particle to distinguish between molecules and solid bodies on a nano-scale length or larger such as soot particles.

An ion wind is generated when a flux of charged species is present in a gas under the influence of an electric field. A single charged species is accelerated by the field in between collisions. The average velocity has been seen to be proportional to the electric field times a constant of proportionality. This average velocity is known as the ion drift velocity and is expressed

as,

$$\mathbf{v_d} = K\mathbf{E}, \tag{2.18}$$

where $\mathbf{v_d}$ is the ion drift velocity vector, K is the ion mobility, and $\mathbf{E}$ is the field strength vector (note: this is the velocity of the ions seen from a reference frame moving with a velocity of the bulk gas).

In general, the transport of charges species is described by the current density and is governed by the ion drift velocity, convection, and diffusion. Thus, charge density becomes,

$$\mathbf{j} = \rho(K\mathbf{E} + \mathbf{V}) - D_i\nabla\rho, \tag{2.19}$$

where $\mathbf{j}$ is the current density vector, $\mathbf{V}$ is the mass average velocity vector of the entire gas, and D_i is the diffusion coefficient. ρ is the charge density (not to be confused with mass density) and is equal to en_i (n_i is the number density of ion species). Macroscopically, the electrical body force per unit volume acting on the entire gas can be described by,

$$\mathbf{F_e} = \rho\mathbf{E}. \tag{2.20}$$

If the contribution of convection and diffusion are assumed to be negligible compared to the ion drift component, then Equation (2.19) can be simplified and inserted into Equation (2.20). This provides a more convenient description of the electrical body force in terms of the current density and the ion mobility.

$$\mathbf{F_e} = \mathbf{j}/K \tag{2.21}$$

It should be noted that $\rho = e(n_+ - n_-)$. Here, $n_\pm$ is the number density of positive and negative charges, respectively, present in the gas per unit volume and e is the charge of an

electron. It is clear that in regions where positive and negative charges coexist the electric body force felt by the entire gas is small. Using this logic, a flame under the influence of an applied electric field feels a very small electric body force and the major effects are felt downstream of the flame where charge separation occurs.

Lawton and Weinberg, [24] et al., used Equation (2.21) with the momentum conservation equation to compute the maximum effects that can be achieved in an ideal scenario. They showed that the current density is limited by the breakdown field of the gas since beyond this point the gas acts as a conductor and the current density is neutralized. They concluded that under ideal conditions, the maximum velocity achievable is 550cm/s in air at s.t.p and assuming H_3O^+ is the strongest contributing charged species to the ion current.

2.2.2 Electric Field Effect

Section 2.2.1 highlighted the electric field effect on gas flows. Many of the effects on combustion when an electric field is applied can be described by this ion wind. Calcote [4] saw a deflection of the flame towards a negative electrode when subjected to transverse electric fields. His conclusion was that the deflection could be explained completely by an ion wind effect. As stated earlier, Bowser and Weinberg compared the burning velocity of burner stabilized flames under the conditions of positive fields, negative fields, and no fields. Heinsohn studied the extinction limits in an opposed jet flame with electric fields [15]. Heinsohn also saw alterations in temperature field using external fields [14]. The application of AC fields to flames has been studied extensively throughout the literature and has produced interesting results. To summarize some main points, ion wind effects are not observed in sufficiently high frequency AC fields. This is because the low ion mobility of positive ions doesn't allow them to travel very far from their location of origin. Thus, the body force on the bulk gas due to ion/neutral collisions is reduced. The ion wind effect has been seen to disappear at

frequencies about 100hz, Karnani et al. [7].

Papac [28] used an electric field to simulate micro-gravity on an inverted capillary jet flame in a ground-based laboratory. However, the author later published a paper showing the net body force acting on bulk gas calculated through simulation is not actually zero everywhere [29]. This is because buoyancy force is determined by a temperature differential while the electric body force is determined by the ion current density. To get these two parameters to match up everywhere in a combustion system is difficult. The simulation avoided the complication of ion chemistry after measuring the ion current and realizing the profile resembled a Warburg distribution. After implementing this into the simulation and assuming the ion current was dominated by a flux of H_3O^+ ions, Papac was able to simulate a flow and temperature field that described very well the effects he observed in experiments. Rickard [33] measured a maximum ion wind velocity of 2.4m/s for a point to ring electrode corona discharge system.

2.2.3 Literature Background Conclusion

EFFD has been studied for over 100 years. Many reviews have been published to summarize many of the conclusions from these studies. The hope of this chapter was to provide a brief summary of the findings that deem significant, at least for the contents in this thesis. This chapter also shows the importance of continued study in EFFD. While many advancements in the knowledge of EFFD have been made in the past 100 years and regardless of the fact that EFFD studies have been less involved within the combustion community in recent decades, a complete understanding is far from realized. This statement includes all areas of EFFD; electric field effects and flame ion chemistry. In order to proceed forward with the practical applications of EFFD, more studies are needed. This thesis focuses particularly on the electric field effects on flames. More specifically, this thesis looks to enhance the

understanding of the dynamical effects on the flow field of the bulk gas due to a flux of electric field driven chemi-ions.

Chapter 3

Experiment

Experiments were designed and conducted to test the interaction between flame produced chemi-ions and the bulk gaseous medium. This chapter explores the different components used in the experiment apparatus, as well as, the conditions under which they were run. The components used in the experiments are divided into three systems; burner & gas flow system, electrical system, and schlieren system. Each system is discussed in detail. Limitations of the conditions are also noted. After the discussion of the systems, an explanation of the actual experiments follow. The experiments are also grouped into three categories; determination of voltage-current curves, high-speed schlieren videos, and high-speed flame videos. The information that is sought out in each experiment will be explained along with its significance. Experimental complications are also addressed in order to provide accurate interpretations of the data.

3.1 Burner

A stainless steel (s.s.) co-flow burner was used in the experiments to produce a laminar, diffusion, jet flame. The co-flow burner consisted of two concentric tubes (see Fig. 3.1). The inner tube had inner and outer diameters of 2.1 and 2.4mm, respectively, while the outer tube had inner and outer diameters of 25 and 38mm, respectively. A 6.35mm thick, s.s., disk was placed in the co-flow annulus, separating the inner and outer tubes. Circular holes were drilled through the s.s. disk in a honeycomb like pattern. The top face of the honeycomb disk sat flush with the top face of the outer tube. From this top face the inner tube was extruded 3mm. Methane was the fuel used and was fed through the inner tube. The methane gas was metered using a rotameter. Air was used as the oxidizer and was metered and fed through the co-flow annulus. The burner was placed inside a acrylic enclosure to shield the flame from any outside disturbances.

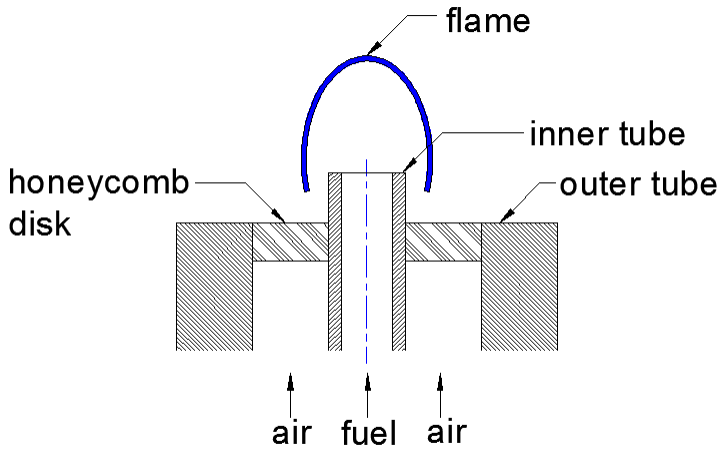

Figure 3.1: Co-flow burner (section view)

3.2 Electrical System

An electric field was externally generated using two 20kV, single output, high-voltage power supply modules with opposite polarities (See Fig. 3.2). The two power supply modules were wired in parallel using a voltage divider that consists of two 100MΩ resistors. The voltage divider was built inside a plastic enclosure and filled with Scotchweld DP270 epoxy for electrical insulation. A resulting ± 10kV variable applied voltage is generated between the electrodes by this electrical system. The dual HV power supply system was controlled with a PC-based, multi-purpose data acquisition. This is represented by the 0-5V near the bottom left corner of the Fig. 3.2. The s.s. co-flow burner described in the previous section was used as the first electrode and a circular, copper mesh was used as the second electrode. This mesh electrode was fixed 3.5cm downstream of the burner electrode for all experiments. This distance was measured from the top face of the honeycomb disk and the mid plane of the electrode mesh.

The spacing of the electrodes is a crucial parameter for this study. Oscillations in flame luminosity and ion currents have been measured and documented in the literature (e.g. Karnani, et al. [18]). Preliminary tests were performed with this electrical/burner system and found that a 3.5cm gap was the minimum distance that the occurrence of these oscillations were found to be minimal (Appendix A). The importance of these preliminary tests was to show that the gap distance may play a role in the combustion process. This is not a well understood relationship and will be the focus of future studies. One hypothesis is that the oscillations is an occurrence relating to secondary ionization. However, in the interests of staying focused on the topic of this thesis, "chemi-ion flow dynamics", a 3.5cm gap was chosen to minimize the oscillations. A large gap distance is also preferable to maintain a large electrode spacing to flame height ratio. Having this ratio sufficiently large will allow for the flame to be modeled as a point source of ions in simulations as was done by Papac [29]. The last consideration for the electrode spacing is to make sure that the electric field

is optimized for the high voltage power supplies, i.e. the "average electric field strength", ($E_{ave} = \triangle V/L$) is related to the inverse of the electrode space, L. Thus, too large of an electrode spacing reduces the maximum field strength that can be generated.

The burner was wired to ground and the mesh electrode was used as the variable electrode. A high voltage probe and a digital multi-meter (both not shown) were used to measure the transient electrode potential between the burner/mesh electrodes. The transient ion current was measured using a 1MΩ shunt resistor wired in series between the burner and ground. 1MΩ was chosen to be sufficiently small compared to the resistance created by the gaseous medium occupying the electrode space region which has been measured to be on the order of 10^9-10^{10} Ω [1]. This shunt resistor was wired inside a plastic enclosure filled with Scotchweld DP270 epoxy. The voltages of both the shunt resistor and high voltage probe were recorded using the data acquisition for analysis.

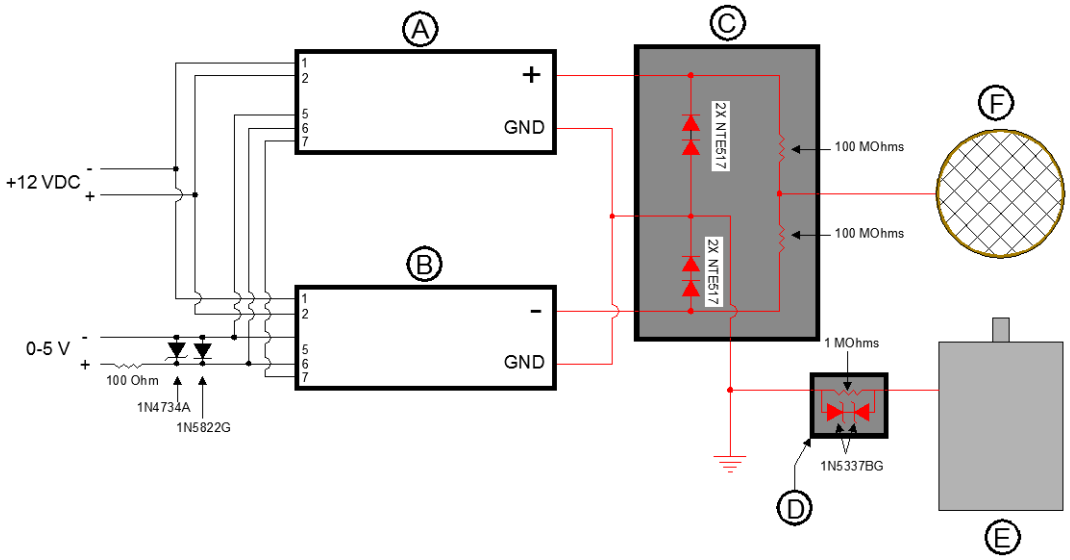

Figure 3.2: Electrical system schematic- item A) positive HV supply module, item B) negative HV supply module, item C) large plastic enclosure containing HV voltage divider (filled with DP270 epoxy), item D) small plastic enclosure containing shunt resistor (filled with DP270 epoxy), item E) stainless steel co-flow burner electrode, item F) copper mesh electrode, components in red symbolize high-voltage electrical components

The electrodynamic properties of the experiment is highly dependent on electrode geometry.

This burner/mesh arrangement was designed with the intention of resembling a simple plane to plane electrode geometry where the electric field lines are quasi-parallel. Since the lines of force of the ion wind act in the direction tangent to the electric field lines, an ideal plane to plane geometry simplifies the analysis of the experiment. However, several issues need to be addressed in this regards.

The first is the case of generating an electric field before considering the presence of a flame. An ideal plane to plane geometry requires two perfectly flat plates placed exactly parallel from each other. Also, the ideal electrodes would require no sharp edges. These have the tendency to produce high local surface charge concentrations which decrease the electrical breakdown potential of the gas within the electrode discharge space. Once the electrical breakdown occurs, secondary ionization mechanisms must be considered and the analysis of the problem becomes complicated. The most obvious example would be the ejection of electrons from the surface of the downstream electrode mixing with the incoming positive chemi-ions within the electrode region. As discussed in Section 2.2.1, this would reduce the electric body force in the region of highest interest.

A copper mesh electrode was chosen as the downstream electrode in favor of a solid flat plate. The limitations related to electrical breakdown for this electrode are based on the wire diameter and wire-to-wire spacing. The disadvantage of using a flat plate as an electrode downstream of the burner is that it creates a stagnation flow within the bulk gas. The effect of a stagnation flow results in a decrease in the maximum velocity that can be produced with an ion wind. A stagnation flow also results in the possibility of recirculating combustion products into the reaction zone. While these are interesting effects in themselves, they are not the desired phenomena to be studied in this thesis.

The second issue arises when a space charge is created by the presence of either ions or electrons in the electrode space. The space charge distorts both the path and the intensity of the electric field lines. This effect is governed by Gauss's Law which can be expressed in

its differential form by,

$$\nabla \cdot \mathbf{E} = \rho/\epsilon_0, \tag{3.1}$$

where $\mathbf{E}$ is the vector form of the electric field strength, ρ is the space charge, and $\epsilon_0 \approx 8.854 \times 10^{-}12$ Farads per meter is the permittivity of free space.

3.3 Schlieren Systems

Lawton and Weinberg described that the most interesting electro-hydrodynamic effects occur outside the reaction zone of the flame [23]. Since the reaction zone is where ion production occurs, both positive and negative charges co-exists, and therefore, the local electrical body force is minimum. The region between just outside of the reaction zone and the electrodes is where positive and negative charges are assumed to be isolated from each other when an external electric field is present. As stated at the end of Chapter 1, one particular goal of this thesis is to study the interaction between ions and bulk gas in the electrode space. However, a challenge arises due to the presence of the electric field.

Many common methods of determining the flow field of a gas (i.e. hot wire anemometry and particle image velocimetry) do not produce reliable data within the electrode space. Kuhl performed experiments using PIV to measure the change in velocity field for premixed flames [22]. The argument against using PIV as a diagnostic method is that seeding particulates into the region of interest runs the risk of the particulates becoming charged themselves [13]. If this were to occur, the particulates would not only gain a velocity different from the velocity of the bulk gas but would also act as low mobility particles that would take part in the ion wind effect. Kuhl did not provide sufficient proof that this was not occurring in his

experiments. Laser Doppler Anemometry (LDA) has the same risks. Signals from hot wire anemometer probes are considerably distorted when placed in the electrode space.

A simple schlieren system was employed in the experiments in order to resolve the issues described above. Schlieren is an optical method that takes advantage of a fluid's refractive index dependence on temperature and pressure. In the case of the experiments described in this text, schlieren was used for visualization of the thermal plume within the electrode space. In the absence of an electric field, the thermal plume is buoyantly driven due to the pressure forces of the cool ambient gas environment acting on the hot combustion gases. The buoyancy force acting on the bulk gas can be described by the Boussinesq approximation $(\rho_0 - \rho)$. The upward motion of hot exhaust gas has been shown to entrain ambient gas horizontally from the environment [9]. With the presence of an electric field, the thermal plume is driven by both buoyancy and electrical body forces. An electrically driven thermal plume has also been shown to entrain ambient gas similar to buoyancy driven thermal plumes but is expected to be on a higher order of magnitude for small flames with low heat release rates. Schlieren is thus a non-intrusive method used to understand how flow field is altered by an electric field.

Fig. 3.3 is a top view of the apparatus. A xenon arc lamp was used as a source for white light. The blue lines represent light rays emitting from the lamp. A lens was used to collimate the light. A converging lens was used to converge the collimated light to the focal point, f.p., and then illuminated onto a movie screen. The flame, represented by the solid gray circle, was placed within the collimated light. Because the index of refraction of a gas is related to density (thus related to $1/T$), the temperature gradient in the hot gas above and around the flame bends the path of the light rays. The dashed blue lines represent these refracted light rays. The angles shown in Fig. 3.3 are exaggerations of the true angles of refraction. A knife edge is placed at the focal point to block a portion of refracted light. Without the knife edge, the displacement of light is too small to produce a noticeable change in light

intensity on the movie screen. The presence of the knife edge is what produces the schlieren image on to the movie screen. The flame is positioned in focus with the converging lense and movie screen to minimize the contributions of shadowgraphy. Thus, the gradient of the intensity of light on the screen is proportional to the first derivative of the index of refraction of the hot combustion gases. The knife edge is positioned so that it is perpendicular to the refractive index gradient of the hot gas medium. For example, if a thin region is assumed, the refractive index gradient could be approximated to be along the y-axis in Fig. 3.3. Then it is most beneficial to position the knife edge parallel to the z-axis coming out of the page. Videos of the schlieren image were recorded with a high-speed video camera at a rate of 1000 frames per second.

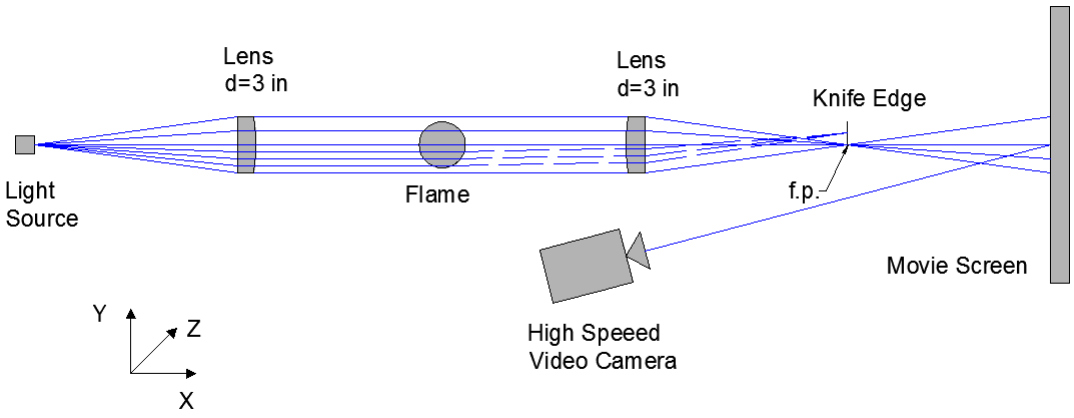

Figure 3.3: Schlieren system: top view

The result of this schlieren system is shown in Fig. 3.4. The burner is seen as a flat surface with a fuel tube extruded 3mm positioned at the bottom of the image. The height of the electrode space is 3.5cm. An LED is placed at the top right of the image. The LED was used to show exactly when the electric field is switched on. The region of interest is the thermal plume inside the electrode gap. The profile of the thermal plume will provide insight into the flow field inside this region. Further details on schlieren can be found in [34] and [41].

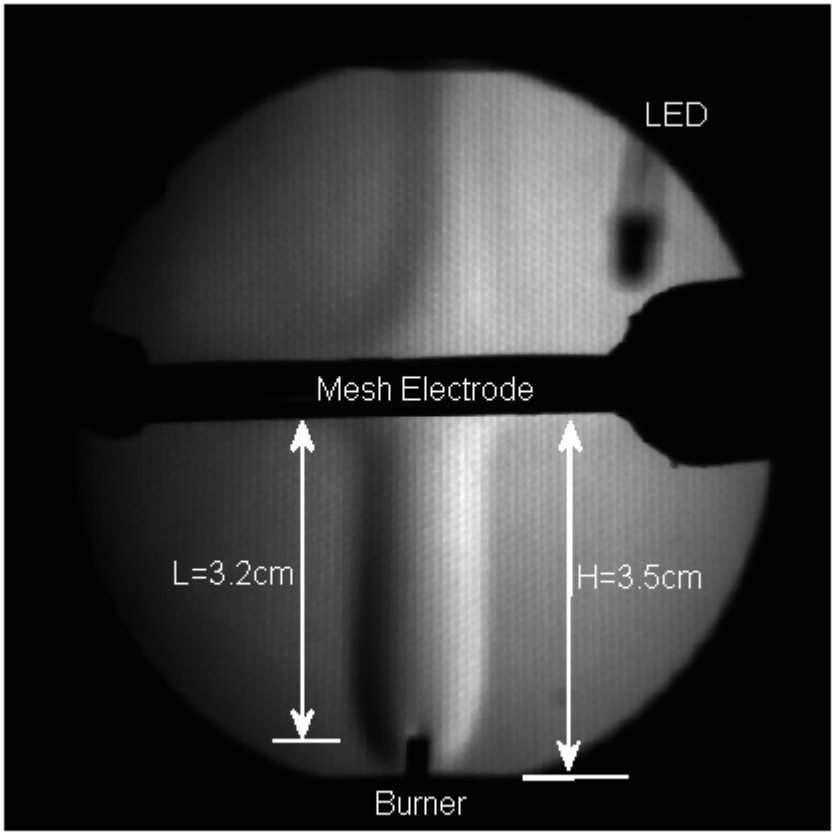

Figure 3.4: Sample schlieren image

3.4 Voltage-Current Characteristics

The first experiment performed in this study was to determine the voltage-current characteristics of the burner/electrical system. This was done by sweeping through the entire ± 10kV range of the HV power supply system and measuring the ion current through the shunt resistor (See Fig. 3.2). At each voltage step, the HV voltage output was held for one second with a sampling rate of 1000 samples per second. After the entire ± 10kV sweep, the measured HV voltage output and shunt resistor current are averaged at each step and

plotted against each other to reveal the voltage current curve.

The first voltage-current characteristic (VCC) was performed without a flame. This was to test whether the electrical breakdown potential ($\triangle V_B$) of the electrode geometry was sufficient enough to obtain reliable data. Considering air as the dielectric gas within the electrode space at ambient temperature and pressure, electrical breakdown is expected to occur at 30kV/cm. However, the electrical breakdown of a gas at elevated temperatures can be approximated to be,

$$E_b = E_{bo}(\frac{T_o}{T}). \tag{3.2}$$

Then the electrical breakdown can be expected to be ≈5kV/cm near flame temperatures. The maximum electrode voltage difference is ±10kV and the electrode spacing is 3.5cm. The maximum average electric field strength is then ≈3kV/cm. This is much less than the electrical breakdown of air at s.t.p. but not when considering flame temperature effects.

If a current is measured in the absence of a flame, then secondary ionization is surely present. The second run was performed with a methane flame. The velocity of methane gas exiting the fuel tube with a 2.1mm diameter was 7cm/s. The purpose of this test was to determine the sub-saturation, saturation, and super-saturation regions as described by Lawton and Weinberg et al., [25]. The results for both cases are shown later in Fig. 4.1 where the average values of the ion current are plotted against their respective average value of applied voltage.

3.5 High-Speed Videos

Section 3.3 described the schlieren system that was built and discussed what type of information schlieren could provide. This section discusses the actual experiment that was

performed utilizing this schlieren system. The fuel was set to a specified flow rate (7cm/s). Relatively low flow rates were chosen for these experiments to reduce the effects that the initial jet momentum has on the flow field downstream from the flame. This will be discussed more in Chapter 4. The co-flow velocity was kept at zero to maintain a quiescent environment around the region of interest. The electrode gap was kept fixed at 3.5cm. A high speed video camera was set at a 14 degree angle from the x-axis as shown in Fig. 3.3.

Initially, the electric field strength was set to zero and at a specified time, the electric field was turned on producing the desired voltage step between the electrodes. The voltage step function is important for understanding the time-scales involved. As can be seen from Equations (2.21) and (2.19), the body force acting on the bulk gas is created by the ion current density. However, the ion current density is proportional to the electric field. For a truly fundamental understanding of the generation of a the electrical body force, the decoupling of the current density from the electric field is essential. Thus, an infinitely fast voltage step function is favored over other time-varying functions such as ramping functions or sinusoidal functions. The high-speed video camera captured the change in the schlieren image during this event. The transient ion current and applied voltage were also recorded during each test. Different tests were performed at different applied voltages with both positive and negative polarities. To complement the schlieren videos, high-speed videos focused on the flame were also captured under the same conditions.

The transient ion current measurements provide insight into time-scales related to the motion of ions. The main points of interest are how long it takes to collect the first current measurements and how long it takes for the ion current measurements to reach its new steady state. The first describes the migration of ions through the electrode space region with an ion drift velocity and the second provides insight into the alteration in ion production at the flame due to the changing conditions.

The high-speed videos of the schlieren image provide insight into time-scales related to ion-

wind. Of interests are the time that it takes the gas to initially react to the sudden application of an external field and how long it takes the fluid to reach its steady state. The first describes how long it takes for the generation of the body force on the bulk gas when compared to the ion current measurements. The body force is generated by the flux of ions and must, therefore, be a function of the collision rate between ions and neutrals. If the collision rate is sufficiently fast than the measurement of an ion current should cause an immediate change in the schlieren profile. Kono [20] predicted this response time to be <10ms while Kuhl [22] saw a response time 2-4ms experimentally. This time-scale is particularly important for the study of applied AC fields. The second time measurement describes how long it takes the body force to reach different regions between the electrodes and how long it takes the gas to stabilize with the changing conditions.

The high-speed flame videos provide insight into time-scales related to combustion-related qualities, such as luminosity, flame shape, soot, etc. Analysis of these time scales will be discussed in the next chapter. Due to the low light emitting flame and fast exposure time of the high-speed camera, quantitative analysis of the videos becomes difficult. Therefore, most of the analysis outside of time-scales will be qualitative. New theoretical models will be proposed in order to complement the physical interpretation of the results.

Chapter 4

Results & Discussion

4.1 Voltage-Current Characteristic Results

Test 1 in Fig. 4.1 shows the voltage current curve without a flame. The result of this test shows that no ionization is occurring due to the geometry of the electrodes. Test 2 shows the voltage current curve with a methane flame flowing with a velocity of 7cm/s out of a 2.1mm diameter fuel tube. A positive applied voltage in Fig. 4.1 represents a positive electric potential applied to the downstream electrode (mesh) with respect to the grounded burner. The electric field is defined as positive when inducing an acceleration of positive charges in the direction away from the burner. Under this definition, a positively charged electrode mesh produces a negative electric field. This is indicated in Fig. 4.1. To the right of 0dV is an increasingly negative electric field and to the left is an increasingly positive field.

The three regions as described in [25], et al., are evident in Fig. 4.1. At zero potential, no current is measured. On the Negative field side, the sub-saturation region is the region between 0 and ≈2kV, where 2kV designates the saturation point. In this region the ion current remains constant at the saturation current. The positive field sub-saturation region

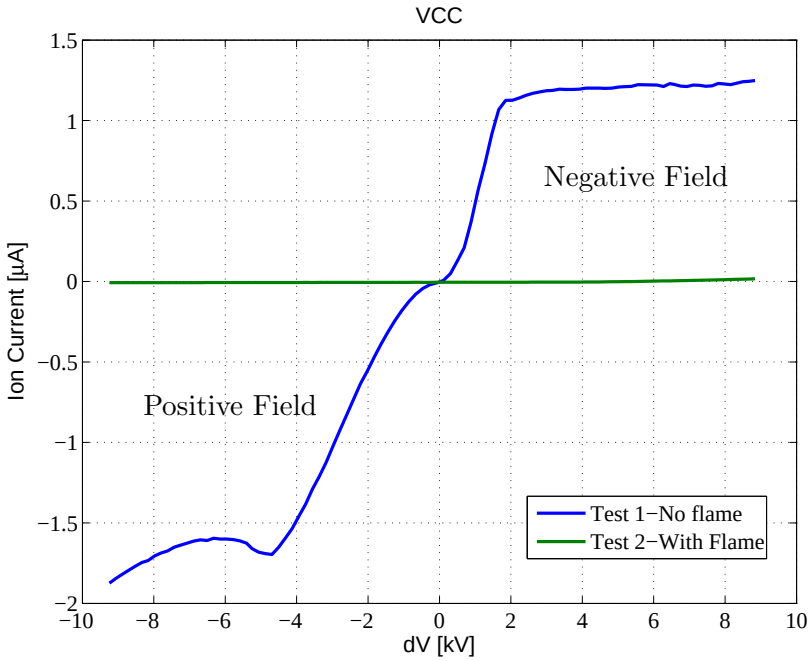

Figure 4.1: Voltage current curve - Test 1) absent flame, Test 2) with flame @7cm/s methane velocity

is the region between 0 and ≈-5kV, where -5kV is again the saturation point. Unlike the negative field case, the current does not remain constant past the saturation point for the positive field. In fact, the current drops shortly after the saturation point and then quickly rises again after -6kV. This is the super saturation region. This variation in ion current suggests that secondary ionization is occurring past the saturation point. Karnani saw this ion current behavior with a similar co-flow jet burner geometry. He showed that this is most likely due to a thermal effect that is giving rise to a secondary ionization effect, i.e. thermionic emission from hot surfaces [17]. Karnani compared the voltage current curve of a methane flame, a hydrogen flame, and no flame in this region, Fig. 4.2. He saw that with no flame, no current was measured. With the hydrogen flame, he measured a current at an applied voltage corresponding to the increasing current in this region. In light of these details, this region will be not be considered in the transient experiments. Further investigation in this region will not be performed in this study since the presence of secondary ionization presents extra complications to the study.

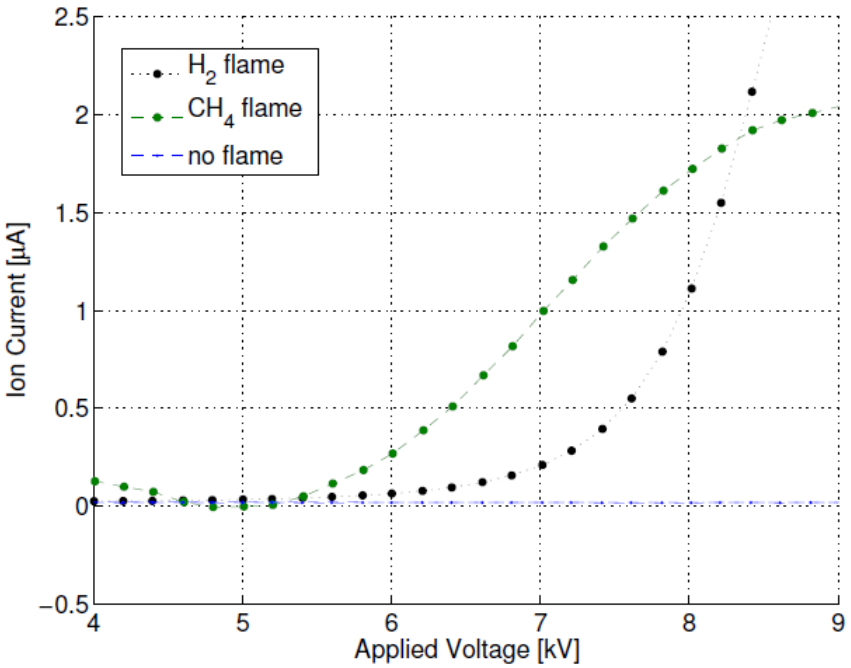

Figure 4.2: Voltage current curve comparison of a hydrogen flame, a methane, and no flame. The methane ion current measurements were reduced by 3μA for visualization of comparison. [17].

4.2 Time-Scale Analysis

Before the results from the high-speed video experiments are shown, a brief discussion on time characterization should be presented. As mentioned in the previous chapter, the measurements gathered will provide insight into the time-scales involved with various processes. Comparing these measured time-scales with time-scales derived from the theory will provide evidence if the theory is in fact correct. Comparing the measured time-scales between different processes will provide clues to the mechanisms involved in those processes, e.g., how soot particles acquire a charge. The purpose of this section is to define characteristic time-scales

.

The first time-scale is the time it takes to pull a charged particle from the flame and retrieve it at the downstream electrode. For a positive field, H_3O^+ is the primary ion thought to exist within the electrode gap as discussed in Chapter 2. Furthermore, the velocity of a single

H_3O^+ ion as it travels through the electrode space is its drift velocity, v_d, which is equal to the product of the mobility of H_3O^+, K_+, and the field strength, E. The time it takes for an H_3O^+ ion to travel from its place of origin, the flame, to the downstream electrode can be approximated by the length of the field line on which the ion travels divided by the drift velocity. Assuming the field strength is constant everywhere on the field line, v_d and the time of flight of an ion, t_{ion}, are,

$$v_d = K_+ E, \tag{4.1a}$$

$$t_{ion} = \frac{L_{EF}}{K_+ E}, \tag{4.1b}$$

where L_{EF} is the length of the electric field line. Since the flame remains attached to the burner, for simplification purposes, it is assumed that the burner and flame have the same potential. It is expected that the charge density only effects the local electric field lines near the flame where the lines are perpendicular to the flame kernel but become parallel quickly downstream in order to become perpendicular to the mesh electrode. This curvature slightly alters the length of the field lines, thus, altering their local magnitude. Since the order of magnitude of this time-scale analysis is what is important, the length of the field line will be taken as the length, a, from the base of the flame up to the downstream mesh electrode. This is a good approximation, since it is thought that the highest concentration of H_3O^+ is located near the base of the flame [17]. The electric field strength will be taken as the average electric field strength. This is defined as the applied electrode potential difference between the two electrodes divided by a. This analysis uses the applied voltage at saturation to produce the maximum, purely chemi-ionization effect. It was shown in the last section that secondary ionization occurs above the saturation voltage. The saturation voltage is

taken from Fig. 4.1. Equations (4.1a) & (4.1b) then become,

$$v_d = \frac{K_+ \triangle V}{a}, \tag{4.2a}$$

$$t_{ion} = \frac{a^2}{K_+ \triangle V}, \tag{4.2b}$$

where a=3.2cm, K_+=2.9cm^2/V$\cdot$ s, and $\triangle V$=5 $\times$ 10^3 V is the applied voltage as measured from the downstream electrode with respect to the burner. The value of K_+ was taken from [38]. Evaluating equations (4.2a) & (4.2b), $v_d \approx$ 4530cm/s and $t_{ion} \approx$ 1ms.

The next time-scale is the time it takes a volume of gas driven by a current of chemi-ions to travel from the flame to the downstream electrode. For simplification, this analysis will use the procedure from [23] for a one-dimensional system neglecting, viscosity, buoyancy, and pressure gradients within the ion stream. The rate of change of momentum along the axis is equal to the body force acting on the gas integrated over the volume between the flame and the downstream electrode. That is,

$$\int_0^A \rho \mathrm{v_z^2 d}A = A \int_0^z (\mathrm{j/K_+}) \mathrm{d}z, \tag{4.3}$$

where v_z is the axial velocity of the bulk gas, j is the ion current density, A is the cross-sectional area normal to the ion stream, and z is an arbitrary location on the z-axis. The gas is assumed to have $\approx$ 0 velocity coming out of the fuel tube. Assuming v_z does not vary within A, j does not vary with z, and then solving for v_z

$$v_{z,ionwind} = \left(\frac{jz}{\rho K_+} \right)^{\frac{1}{2}}. \tag{4.4}$$

The time it takes a volume of bulk gas to travel from the flame to a point along the z-axis

can be described as

$$\int_0^t \mathrm{d}t = \int_0^a 1/\mathrm{v_z}\,\mathrm{dz}. \tag{4.5}$$

Taking the ion current at saturation, density that of air at ambient temperature, and the ion mobility of H_3O^+, Equation (4.5) becomes

$$t_{ionwind} = 2\left(\frac{\rho K_+ a}{j_s}\right)^{\frac{1}{2}}. \tag{4.6}$$

Evaluating Equations (4.4) & (4.6) at z=a=3.2cm, it is found that $v_{z,ionwind}$ = 187cm/s and $t_{ionwind}$ = 34ms, respectively. That is, the maximum axial velocity of a gas being driven by a flux of chemi-ions occurs at the downstream electrode and is expected to reach ≈180cm/s. This is much lower than the 550cm/s that was computed by Lawton and Weinberg in [23]. For their analysis, the field strength was limited by the electrical breakdown field of air at s.t.p., 30kV/cm. This is the ideal theoretical maximum values for ion wind effects. In a combustion system, temperatures above s.t.p. lowers the breakdown field as stated in Equation (3.2). Therefore, elevated temperatures decrease maximum velocity of the bulk gas. On the other hand, the values used in the analysis presented here are being limited by the saturation field which was measured experimentally. It's well documented that saturation currents are proportional to the fuel flow rate, [7] et al. Increasing the flow rate would increase the saturation field unless the saturation field is greater than the breakdown field. It would then seem more logical to study the ion wind at higher flow rates until just before breakdown. The argument against using higher flow rates is that it increases the velocity contribution from the initial jet momentum.

While the maximum velocity is useful for comparing this study with those from the literature, an average axial velocity is also usefel for comparison with the results in the upcoming

sections. That is,

$$\begin{aligned} \overline{v}_{z,ionwind} &= \frac{1}{a}\int_0^a \mathrm{v_{z,ionwind}}\,\mathrm{dz} \\ &= \frac{2}{3}\left(\frac{j_s a}{\rho K_+}\right)^{\frac{1}{2}}, \end{aligned} \tag{4.7}$$

where $\overline{v}_{z,ionwind}$ is the average axial velocity when integrated along the entire length between 0 and a. It is seen that the average velocity is two thirds of the maximum velocity. This results in a velocity of 124cm/s. Using this average velocity, the time it takes a volume of bulk gas to travel from the flame to the downstream electrode can be approximated by dividing length a by $\overline{v}_{z,ionwind}$. The result is,

$$\bar{t}_{ionwind} = \frac{3}{2}\left(\frac{\rho K_+ a}{j_s}\right)^{\frac{1}{2}}. \tag{4.8}$$

Evaluating Equation (4.8), $\bar{t}_{ionwind} \approx 25$ms. (Note that this average flight time is less than the time calculated from Equation (4.6) since it is assuming a constant velocity while Equation (4.6) is taking into account a gradually increasing velocity starting from rest).

The final time-scale is the time it takes for a buoyantly driven volume of gas to travel from the flame to the downstream electrode. The velocity of a buoyantly driven gas can be approximated by,

$$v_{z,buoy} = \sqrt{g\beta(T - T_\infty)z}, \tag{4.9}$$

where $g = 9.81 m/s^2$ is the acceleration of gravity, β is the thermal expansion of gas within the electrode space, T is the local gas temperature, and T_∞ is the ambient temperature. Equation (4.9) was derived from a simplified, one-dimensional momentum equation using the Boussinesq approximation for the buoyancy force. Furthermore, for an ideal gas,

$$\rho = \frac{P}{RT}, \tag{4.10}$$

$$\beta = -\frac{1}{\rho}\left(\frac{\partial \rho}{\partial T}\right)_P = \frac{1}{T}. \tag{4.11}$$

After inserting Equations (4.11) and (4.10) into (4.9),

$$v_{z,buoy} = \sqrt{g\left(1 - \frac{T_\infty}{T}\right)z}. \tag{4.12}$$

The time it takes a volume of bulk gas to travel to any point along the z-axis can be described by,

$$\int_0^t \mathrm{d}t = \int_0^a \frac{1}{\mathrm{v_z}}\,\mathrm{d}z. \tag{4.13}$$

Integrating Equation (4.13),

$$t_{buoy} = 2\left(\frac{a}{g\left(1 - \frac{T_\infty}{T}\right)}\right)^{\frac{1}{2}}. \tag{4.14}$$

By taking $T \approx 1800K$, $T_\infty = 298$K, and $z = a = 3.2$cm, Equations (4.12) and (4.14) gives a maximum velocity $v_{z,buoy} \approx 50$cm/s and $t_{buoy} \approx 125$ms, respectively. Using an average as was done for the ion wind velocity,

$$\overline{v}_{z,buoy} = \frac{2}{3}\sqrt{g\left(1 - \frac{T_\infty}{T}\right)z}, \tag{4.15}$$

$$\bar{t}_{buoy} = \frac{3}{2}\left(\frac{a}{g\left(1 - \frac{T_\infty}{T}\right)}\right)^{\frac{1}{2}}. \tag{4.16}$$

The results of Equations (4.15) and (4.16) are 34cm/s and 90ms, respectively.

Table 4.1 summarizes the results from this section. The average values of the velocities and time-scales are used in the table. These results will be compared in the following section.

The maximum velocities could be used to compare to the ideal maximum of 550cm/s as determined by Lawton and & Weinberg.

Velocity	Time
$v_d > 1000$cm/s	$t_{ion} \approx 1$ms
$v_{z,ionwind} > 100$cm/s	$t_{ionwind} \approx 30$ms
$v_{z,buoy} > 30$cm/s	$t_{buoy} \approx 100$ms

Table 4.1: Characteristic velocities and time-scales for ion drift, ion driven wind, and buoyant driven wind

4.3 Transient Results

4.3.1 Power Supply Performance

Fig. 4.1 was used to determine what applied voltage ranges are most appropriate for studying purely chemi-ion driven flows. It can be seen from Fig. 4.1 that 0 to -5kV is the best range for studying a positive field and 0 to +2kV is best for studying a negative field. Actually, applied voltages slightly above +2kV are also acceptable for the negative field since there were no indication of secondary ionization. For the sake of consistency, the saturation points for both positive and negative fields were used for examination of the transient portion this study.

Fig. 4.3 shows the applied voltage and current measurements versus time measured without a flame for both positive and negative fields. This was to test the high-voltage power supply's ability to deliver charge to the electrode in order to raise the electric potential. The applied voltage command was programmed using Labview to produce an instantaneous 0 to -5kV step function at t_o=0ms for a positive field. Fig. 4.3(a) shows that the high-voltage power supply has a relatively slow step response. The applied voltage has an initial ramp to just over -4kV with a slope of approximately -0.27kV/ms. After this peak, there is a slight

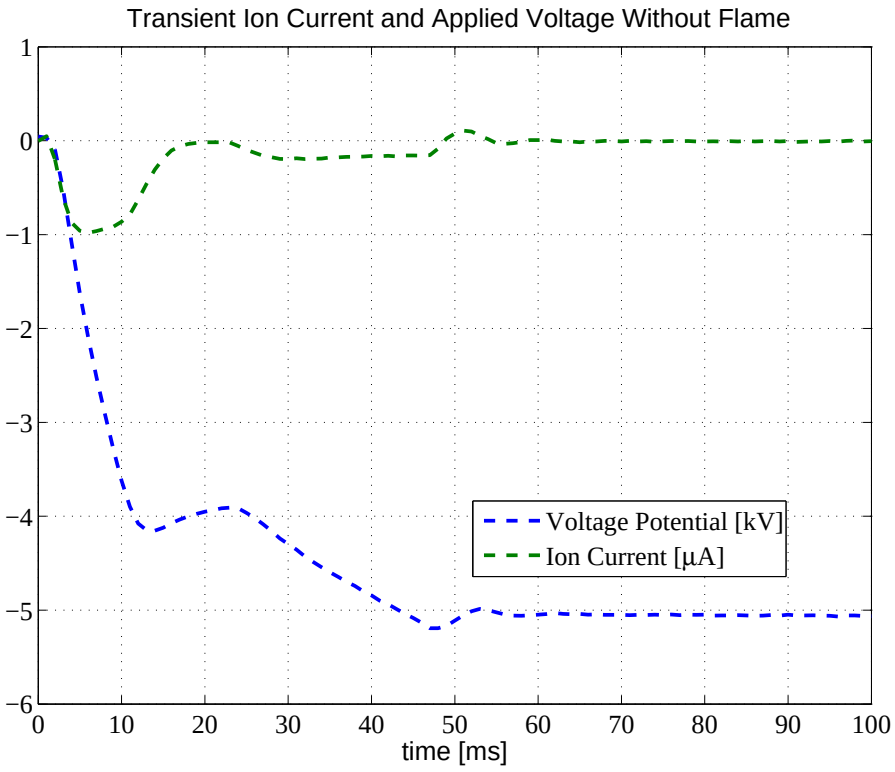

(a)

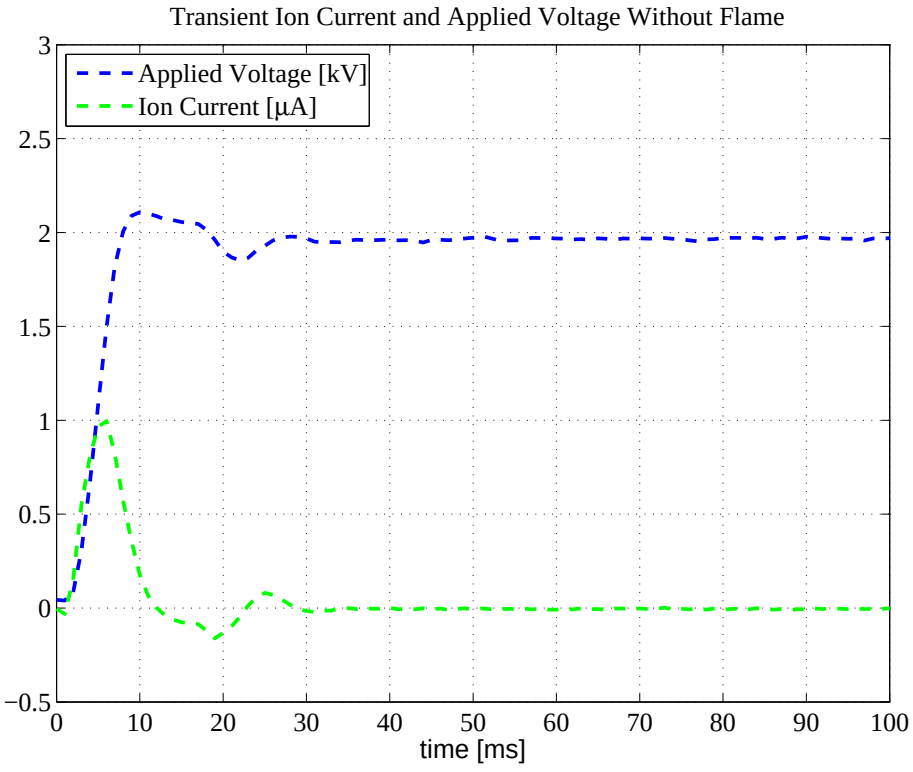

(b)

Figure 4.3: Transient voltage and current response to a step voltage command without flame: (a) positive field (b) negative field

decrease in the applied voltage followed by a second ramp to -5kV at a rate of -0.04kV/ms. At ≈55ms after the initial step function command the applied voltage finally settles to -5kV. The current measured from the shunt resistor showed some current measured through the electrical system. This was the current needed to raise the electric potential of the electrode. An initial spike in current is needed to create the initial rise in applied voltage to -4kV between t=0 to 20ms. A second current is measured corresponding with the current needed to charge the electrode from -4kV to -5kV. The current settles back to zero after 55ms from the initial step function command.

The applied voltage command for the negative case was programmed to produce an instantaneous 0 to 2kV step function at t_o=0ms. Fig. 4.3(b) shows a better response time than the positive field. The applied voltage ramps to 2kV approximately 10ms after the step command is initiated. The applied voltage then settles at ≈30ms. Similar to the current in Fig. 4.3(a), a measured current is shown in Fig. 4.3(b) corresponding to the current supplied by the power supply to charge the electrodes. The current settles to zero after 30ms from the initial step function command.

At this point it is worth making a comment in defense of the power supply system used in this study. The desire for an instantaneous step function is necessary for completely decoupling the ion current response from the applied voltage response. This was discussed in Section 3.5. However, it is clear from Figs. 4.3(a) and 4.3(b) that the high voltage power supply does not have this capability. This makes evaluation of the time-scale related to the ion motion (also discussed in Section 3.5) difficult to perform. From Section 4.2, the expected time-scale for the ion current is ≈ 1ms. Then a power supply that is capable of producing a step voltage much quicker than 1ms is desired.

The important question of this study is related to the generation of a chemi-ion driven wind. Decoupling of an ion-driven wind from a buoyancy-driven wind is much more challenging than decoupling of current and voltage measurements in an electrical system. The answer to

this challenge of decoupling the body forces has been proposed for micro-gravity experiments where the buoyancy force created by variations in gas temperatures are negligible. In fact, this research group is currently preparing for micro-gravity experiments on board the International Space Station via Advanced Combustion Micro-gravity Experiments (ACME) with the cooperation of NASA Glenn. The power supply system used in this thesis was originally chosen for ACME due to its low-cost, compactness, and low EMI emissions; the latter being the primary deciding factor. Other power supplies with higher output power ratings fail this EMI requirement and were determined to not be suitable for use on the ISS. That being said, the experiments described in this thesis serve as a preliminary study for the experiments to be performed on the ISS. Performing these experiments with this particular power supply is necessary with this in mind. Proper characterization of this HV power supply system can be done by creating a transfer function as was done by Borgatelli [1]. The characterization of the power supply is necessary to distinguish between the ion current collected and system current provided to handle the electric potential loading at the electrodes. The performance of this power supply will be taken into consideration for the rest of this study.

The same applied voltage step function commands from Fig. 4.3 were performed with a flame. Figs. 4.4(a) and (b) shows a comparison of two cases for both a positive and negative field, respectively. The dashed lines are the cases having no flame and solid lines the cases with a flame. Similar profiles appear between the case of no flame and the case of with a flame.

For the positive field case (Fig. 4.4(a)), the measured applied voltage is slightly altered after the 10ms mark. This is most likely due to the fact that the power supply has to now supply sufficient current to the electrodes to raise the electric potential and also to neutralize the incoming positive ions. The ion current measurement is increased to $\approx 2\mu A$. The variation from this measured value after 10ms is easily seen to be caused by the performance of the power supply. In light of this, the time it takes to collect a steady stream of ions at the

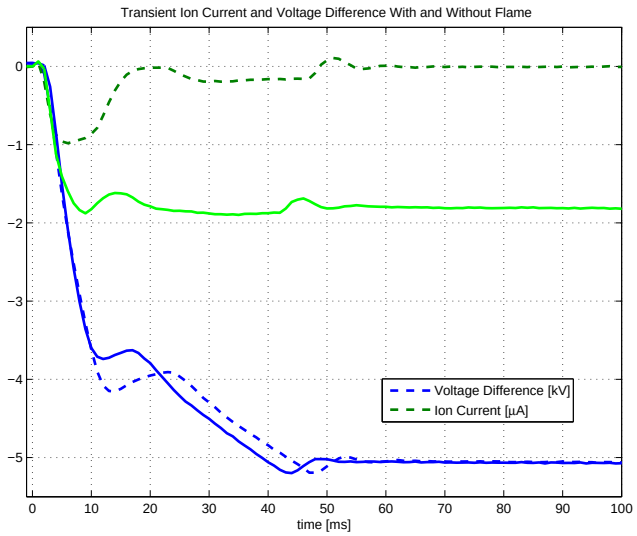

(a)

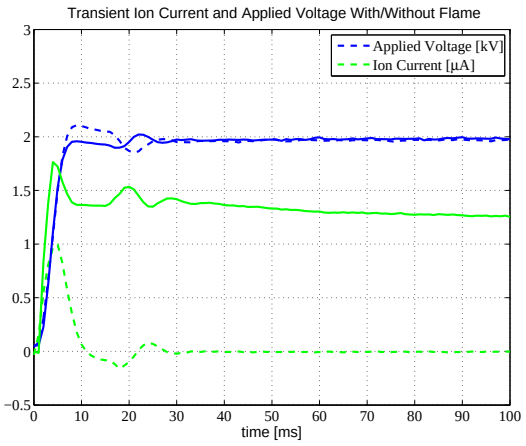

(b)

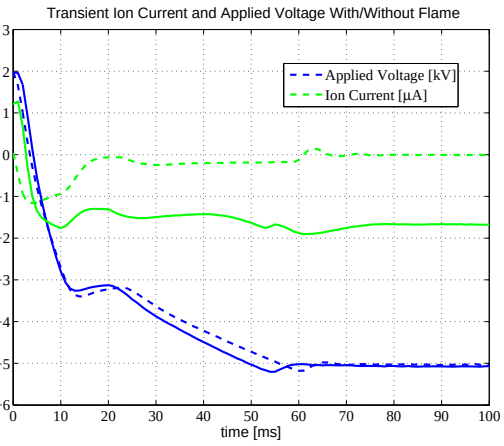

(c)

Figure 4.4: Comparison between w/flame (solid lines) and w/o flame (dashed lines) for transient voltage/current response to a step voltage command: (a) positive field, (b) negative field, (c) negative to positive field.

downstream electrode is ≈10ms. After 10ms, the ion current is considered to be steady.

The complication of the slow power supply is easily seen. As discussed in Section 4.2, the time of flight of an ion through the electrode region is on the order of 1ms. However, Fig. 4.4(a) shows that not all the ions are arriving downstream at this time-scale. One hypothesize is that the ions form a neutral cloud around the flame and shields the flame from the electric field. The introduction of a field would then need some time to peel the layers of the ion sheath since the coulomb force is only able to act on the ions closest to the edge of the sheath. An easily-relatable analogy is a line of cars at a red light. When the light turns green, it is possible for every car to increase their speed in one unified motion. However, the reality is every car waits for the car ahead of it to move before it begins its own acceleration. In this analogy, the cars play the role of the ions and the red light plays the role of the initiation of the electric field. Another possibility is that locally the electric field is not changing uniformly because of the slowly rising electric potential. More analysis is needed in order to determine the cause.

A similar story occurs for the negative field case (Fig. 4.4(b)). The measured voltage has slightly lower initial peak but settles approximately the same time. The measured current has an initial rise to a peak current ≈1.75μA before dropping just below 1.5μA. After ≈30ms, the current begins a slow gradual decrease that lasts much longer than any of the expected time-scales.

Fig. 4.4(c) shows a applied voltage step command extending from the limits of a negative field to a positive field. This figure shows that a negative to positive field step function bares a resemblance to the 0 to positive field step in Fig. 4.4(a) .

As a final comment to conclude this discussion on the power supply performance is to note that, while the applied voltage measurements are slower than ideal, the ion-current measurements are shown to be relatively fast indicating that an ion-current is quickly becoming

established within the electrode gap. This provides some assurance that the data collected from these experiments are worth analyzing since, after all, it is the interaction between chemi-ions and bulk gas that is the main focus of investigation. Therefore, the ion current measurements provide the more interesting information than the electric field measurements.

4.3.2 Positive Field

Snapshots from the high-speed schlieren video can be seen in Fig. 4.5 at different instances in time after the power supply is switched on. The LED determines this instant (t_o=0ms). Fig. 4.6 is a plot of the voltage/current measurements versus time taken during the video. In Fig. 4.5(a), the thermal plume starts at steady state where the gas velocity is driven only by buoyancy forces in the hot gas. At this state, the plume boundary has ≈12mm diameter thickness downstream of the burner. The base of the plume boundary covers most of the extruded fuel tube. After the electric field is switched on, no noticeable movement occurs in the plume boundary until t=10ms. It should be noted that by comparison to Fig. 4.6, the ion current has become fully established just a few milliseconds prior to the 10ms mark. This shows that the interaction between chemi-ions and bulk gas occurs on the order of <10ms. This is slightly faster than the 14ms prediction of Kono [21] and agrees more or less with Kuhl's findings [22].

At the instant of first noticeable motion, the base of the plume slowly rises and the diameter of the plume begins to decrease as if it was being squeezed by an outside pressure. This movement initiates a wave-like motion in the plume boundary that propagates downstream as can be seen in Figs. 4.5(b) - (e). In Fig. 4.5(c), the thermal plume appears to have two distinct cloud regions; an upper, "buoyancy-driven" cloud and a lower, "ion-driven" cloud. The "ion-driven" cloud is the region in the thermal plume where the electrical body force has become established and is effectively driving the bulk gas downstream. The increase

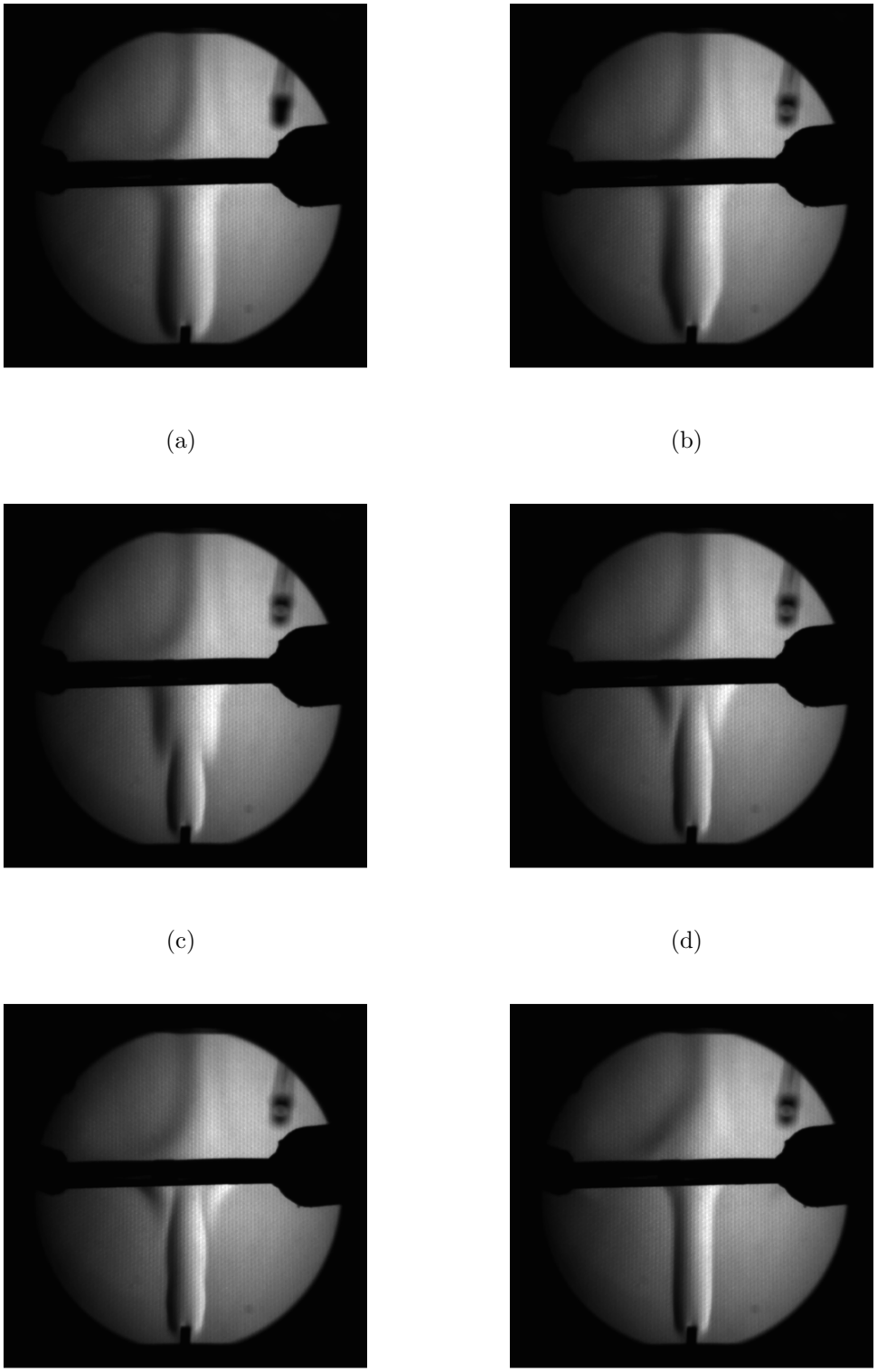

(a) (b)

(c) (d)

(e) (f)

Figure 4.5: Snapshots taken from high-speed schlieren video (positive field): (a) t<0ms, (b) 24ms, (c) 43ms,(d) 52ms, (e) 56ms, (f) 90ms.

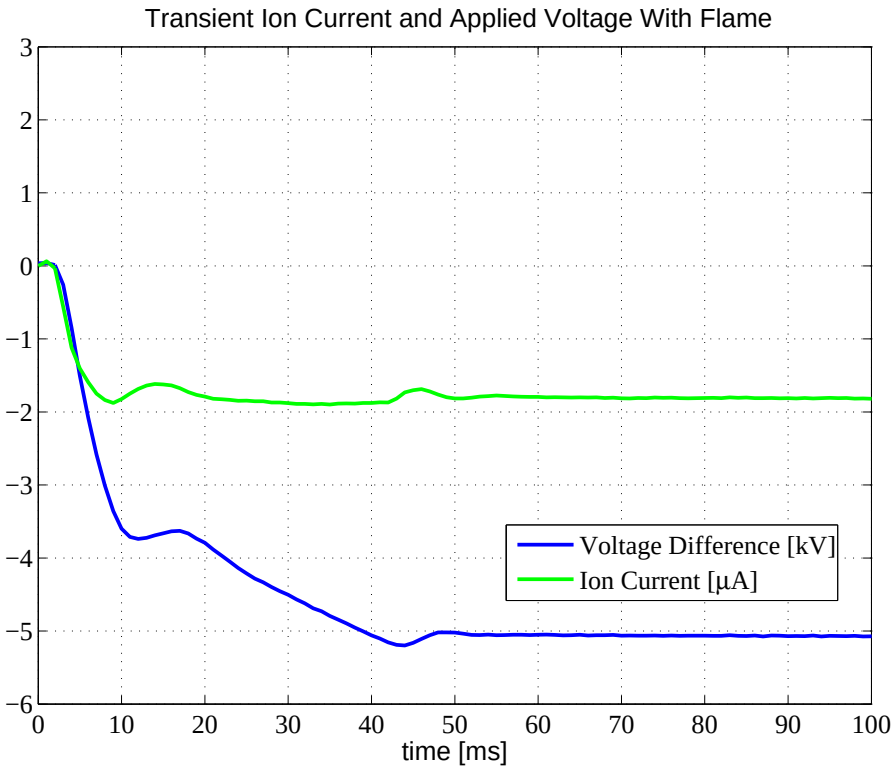

Figure 4.6: Transient voltage/current measurements corresponding with Fig. 4.5.

of axial velocity induces an entrainment of cool gas from the ambient environment which is the cause of the reduction in the plume diameter. The plume diameter is determined by the inward radial convection of cool entrainment gas balancing with the outward radial thermal/mass diffusion of hot combustion gases. While the velocity profile is quantitatively undetermined, the profile of this "ion-driven" cloud can be seen to over take the "buoyancy-driven" cloud around 40ms. The slower, "buoyancy-driven" cloud is forced outward, creating a "winged-shaped" profile as seen in Figs. 4.5(c) & (d). Around 50ms, a second wave-front forms which can be seen as a small ripple in Fig. 4.5(e). This secondary wave is most likely due to the stabilization of the flame where the parameters influencing combustion have been altered by the change in the hydrodynamics near the flame. This will be discussed in the upcoming paragraphs. After the second wave passes the downstream electrode, the thermal plume reaches a new steady state ≈90ms after the electrical field was switched on. This new thermal plume profile can be seen in Fig. 4.5(f). The final plume boundary diameter is

≈8mm.

The time it takes this first wave to travel from the fuel tube to the downstream electrode is ≈50ms minus 10ms, the latter being the instant of initial movement. The average velocity of the wave is then t =3.2cm/0.040s=80cm/s. This plume wave velocity is slightly slower than the 127cm/s predicted by equation (4.7). This may be a result of the slow time response of the HV power supply as discussed in the previous section. However, as mentioned earlier, the ion flux through the gap space appears to be well established as indicated by the ion current measurement. Another hypothesis is the velocity of the wave is being impeded by the slower moving gas immediately downstream of the wave. Another possibility is that the local electric field is not constant throughout the electrode gap as was assumed in Section 4.2. This is not a new hypothesis but rather an agreed upon fact through out the EFFD community, e.g., [42].

Before proceeding further, a brief comment should be made about the terms "ion-driven" and "buoyancy-driven" clouds. These two terms are being used loosely in this text since it is clear that these two driving body forces are not decoupled in the experiment. Emphasis is once again placed on micro-gravity experiments where the electrical body force can be studied in isolation from buoyancy. One goal for a near-future analytical study will be to perform dimensionless analysis on chemi-ion driven flows using methods analogous to purely buoyancy driven flows, which is much more well understood. This future study will determine scaling laws for combustion that is influenced by an external electric field. The concept is to define a Grashof number based on electro-hydrodynamic parameters. A comparison of a buoyancy-based Grashof number and an electric field-based Grashof number will determine the effectiveness of electric field combustion at different scales and applications. Micro-gravity experiments will aid in this study.

Fig. 4.7 shows snapshots taken from the high-speed flame videos. These videos were added to compliment the schlieren videos since readers are more accustomed to flame images than

schlieren images. The flame video was recorded at a different instant than the schlieren video since the high-speed frame rate and low exposure times make it difficult to record both simultaneously. Fig. 4.8 was added as proof of repeatability as far as electrodynamics is concerned. It can also be shown that results of both schlieren and flame videos are easily repeatable. Therefore, the schlieren and flame videos are compared together without question.

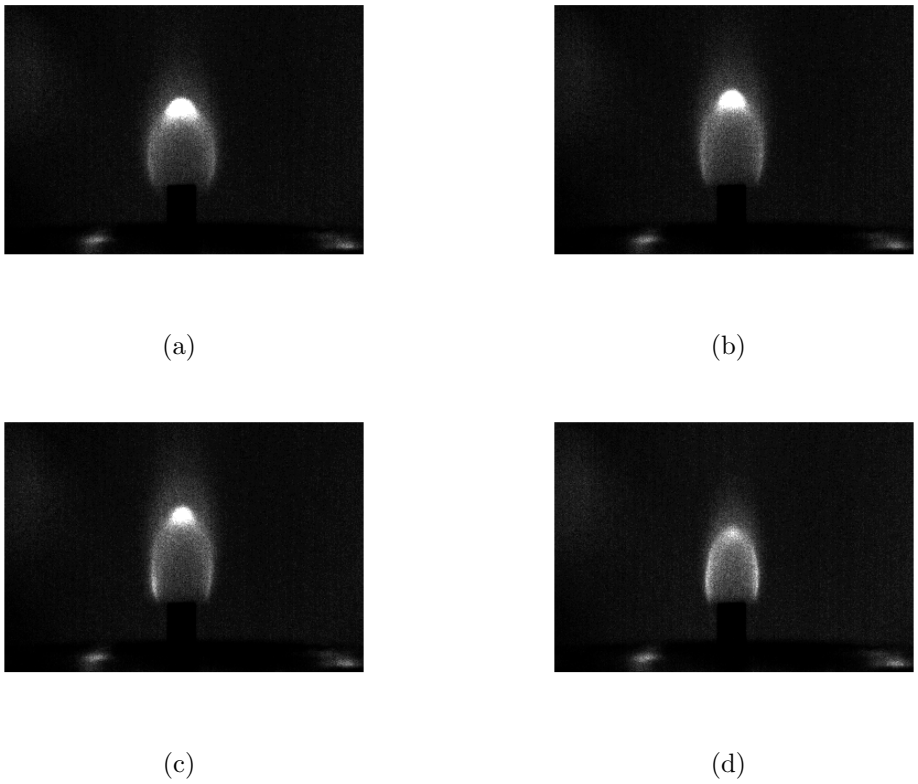

(a) (b)

(c) (d)

Figure 4.7: Snapshots taken from high-speed flame video (positive field): (a) t<0ms, (b) 16ms, (c) 19ms,(d) 45ms.

Fig. 4.7(a) shows the flame in its initial steady state. The video was taken in black and white video, but its easy to imagine the flame as a typical blue, egg-shaped, methane flame. A soot region is present at the tip of the flame which is seen as the white glowing region. Again, the electric field voltage step function is switched on at t=0ms. The first noticeable change occurs at $t \approx$8ms. At this instant, the flame structure is stretched along its axial

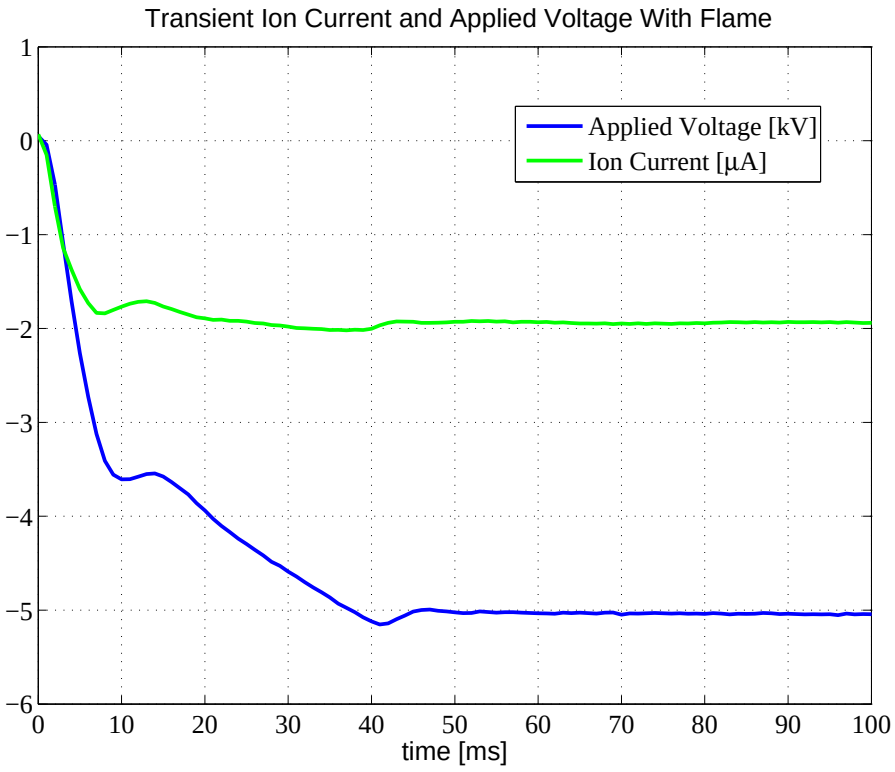

Figure 4.8: Transient voltage/current measurements corresponding with Fig. 4.7.

length causing the height to increase and the diameter to decrease. This stretching is best described by an ion wind effect. The mechanical drag by ions increases the axial velocity of the bulk gas. The stretching causes entrainment of gas from the environment radially. This explanation agrees with the effects seen in the schlieren video where the first changes in the schlieren boundary are seen at t=10ms. At ≈16ms, the flame height reaches a maximum as seen in Fig. 4.7(b). After this maximum, both the flame height and diameter decrease to a new state. As this change occurs, the soot region nearly disappears completely. In Fig. 4.7(c), an interesting effect begins to occur. An increase in luminosity originates at the base of the flame. In Fig. 4.7(c), this can be seen as the the intensified glow at the flame base. In this image, this intensified glow is more noticeable near the lower left side of the flame. The intensified glow quickly engulfs the entire flame. When compared to the schlieren video, this intensified glow begins at ≈19ms which is approximately the time it takes the thermal plume boundary to shrink in this local region. The intensified glow could

then be explained by the higher local concentration gradient of combustion reactants near the flame resulting in a more intense combustion reaction. It is also easy to imagine that the flame could be entraining air from below the flame. The final flame structure is much more compact, luminous, and soot free than the original state as seen in Fig. 4.7(d). The flame reaches this new state in ≈45ms.

4.3.3 Negative Field

Snapshots from high-speed schlieren video with a voltage step producing a negative field are shown in Fig. 4.9. Fig. 4.9(a) shows the thermal plume in its initial state before the electric field is turned on. The initial plume diameter is consistently ≈12mm downstream of the burner. At t_o=0ms, the electric field is turned on. The first noticeable movements occurs at ≈9ms. The base of the plume drops lower than its inital height becoming attached to the top of the honeycomb surface. As this happens, the diameter of the plume boundary near the fuel tube widens as the diameter further downstream thins. The final plume profile is achieved at ≈90ms and can be seen in Fig. 4.9(c). The lower portion of the plume is wider and rounder than the upper portion. The widest diameter of the lower portion is ≈13mm while the upper portion has a diameter of ≈10.5mm.

For a negative field, the positive ions are pulled toward the burner while electrons are pulled downstream. Near the flame, the positive ions are forced to collide with the gas exiting from the fuel tube. This decreases the axial velocity of the bulk gas in this region which explains the widening of the plume boundary near the flame. Further downstream, the plume boundary is thinner. An ion-wind effect is occurring in this region due to the flux of electrons being collected at the downstream electrode. The ion-wind effect due to electrons is not as significant as seen with positive ion due to electron's higher mobility. The transient applied voltage and current measurements taken during this video is shown in Fig. 4.10

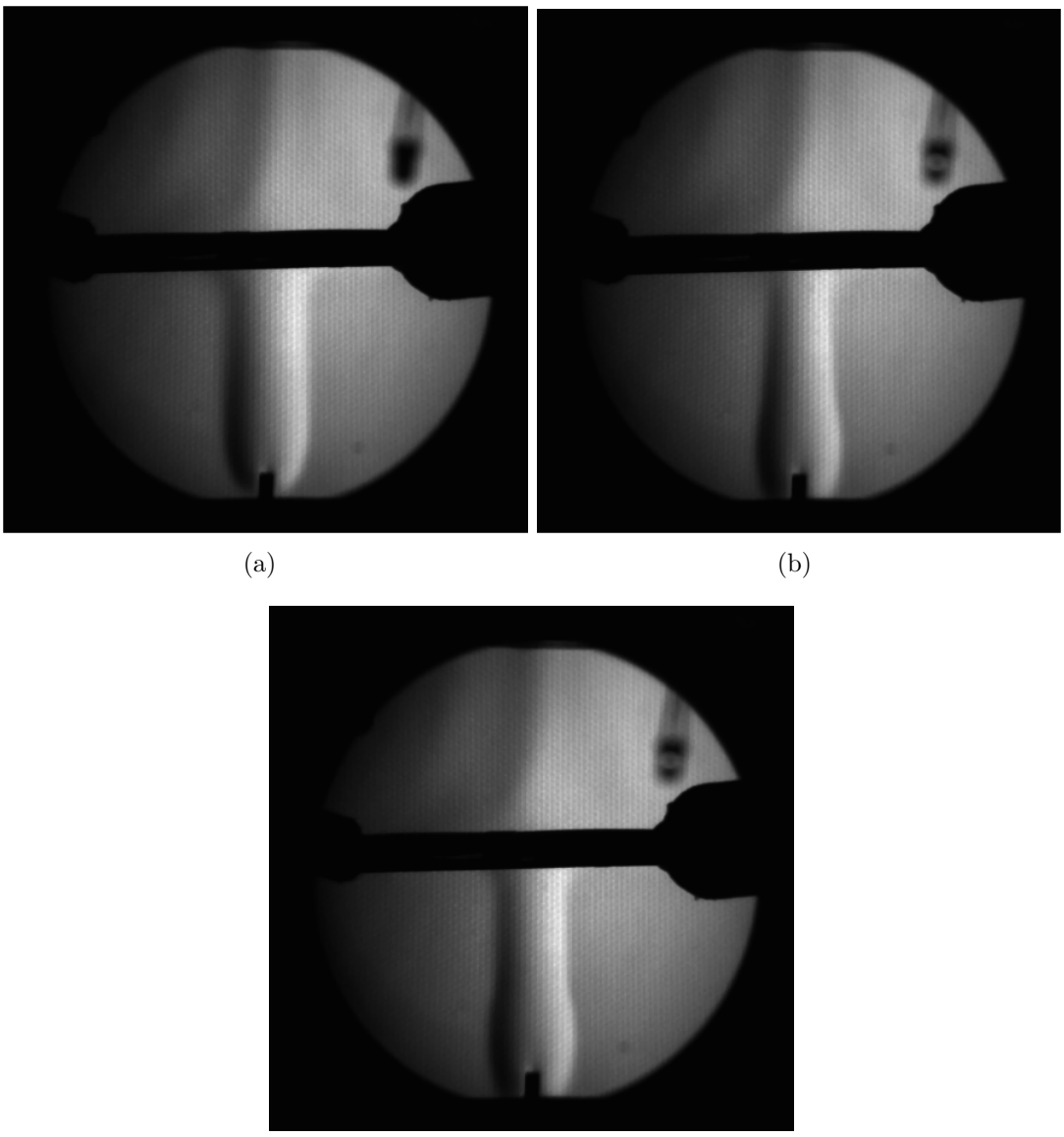

(a) (b)

(c)

Figure 4.9: Snapshots taken from high-speed schlieren video (negative field): (a) t<0ms, (b) 63ms, (c) 92ms.

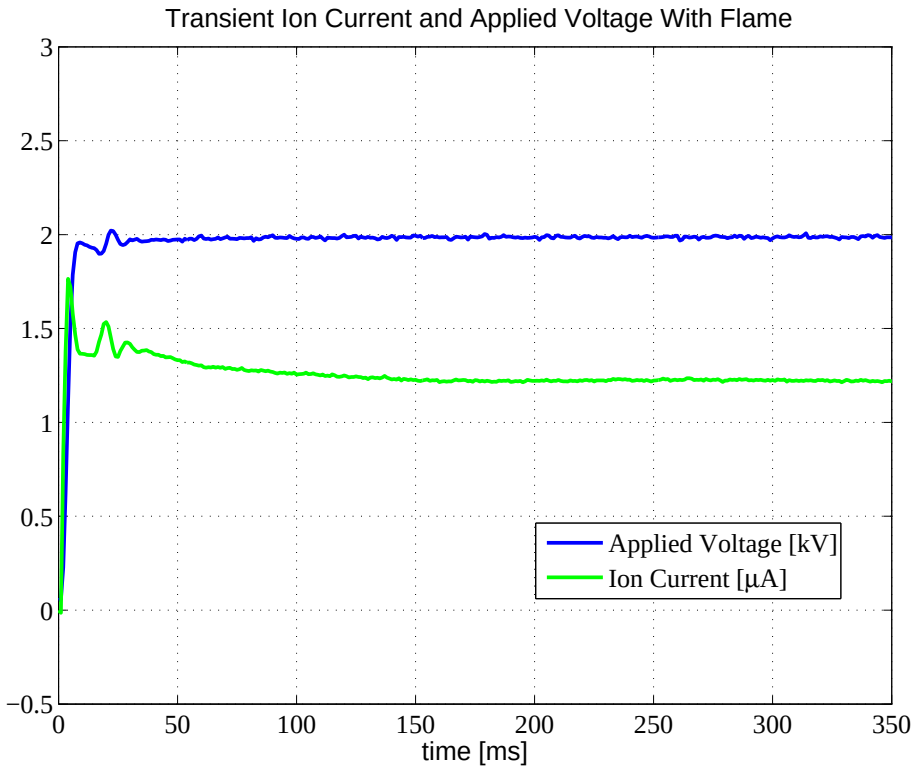

Figure 4.10: Transient voltage/current measurements corresponding with Fig. 4.9.

Snapshots taken from the high speed video of the methane flame during a negative field step is shown in Fig. 4.11. The video shows the flame at its initial state before the electric field is switched on in Fig. 4.11(a). It takes ≈8ms for a noticeable change in the flame structure. The initial change shows the flame height decrease as the diameter increases. As this happens, the glowing soot region increases as can be seen in Figs. 4.11(a)-(c). Around 40ms the flame reaches a minimum height and then reverses direction: Figs. 4.11(c)-(d). The flame structure continues to expand till ≈130ms where its final shape is formed; Fig. 4.11(e). The soot region was also seen to drastically decrease between Figs. 4.11(c)-(e). In fact, the soot region continues to decay very slowly even after the flame structure has reached its final shape. This slow decay ends ≈350ms after the electric field was initially turned on. The final state of the flame has a larger surface area and is less luminous than the original state. Visual traces of soot have completely disappeared. It is also interesting to point out that the slow decay of the soot region corresponds extremely well with the slow

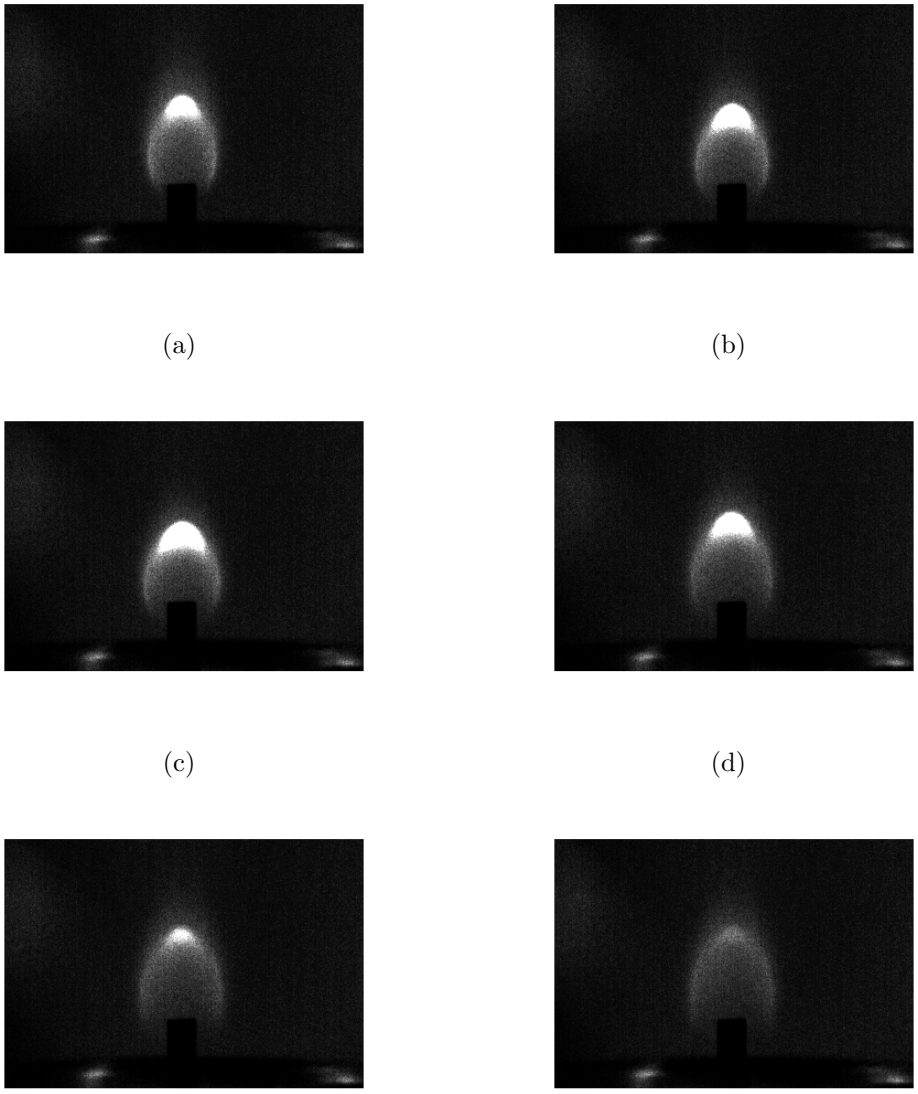

(a) (b)

(c) (d)

(e) (f)

Figure 4.11: Snapshots taken from high-speed flame video (positive field): (a) t<0ms, (b) 25ms, (c) 40ms, (d) 82ms (e) 136ms,(f) 324ms.

decay in ion-current measured which can be seen in Fig. 4.12. The overall flame shape has more of a "half-egg" shape compared to the initial shape.

There have been studies dating as far back as the 1950's dealing with the relationship between soot and the electrical properties of flames. It has been demonstrated that soot particles do acquire charge. When and how these particles acquire charge has been one topic of

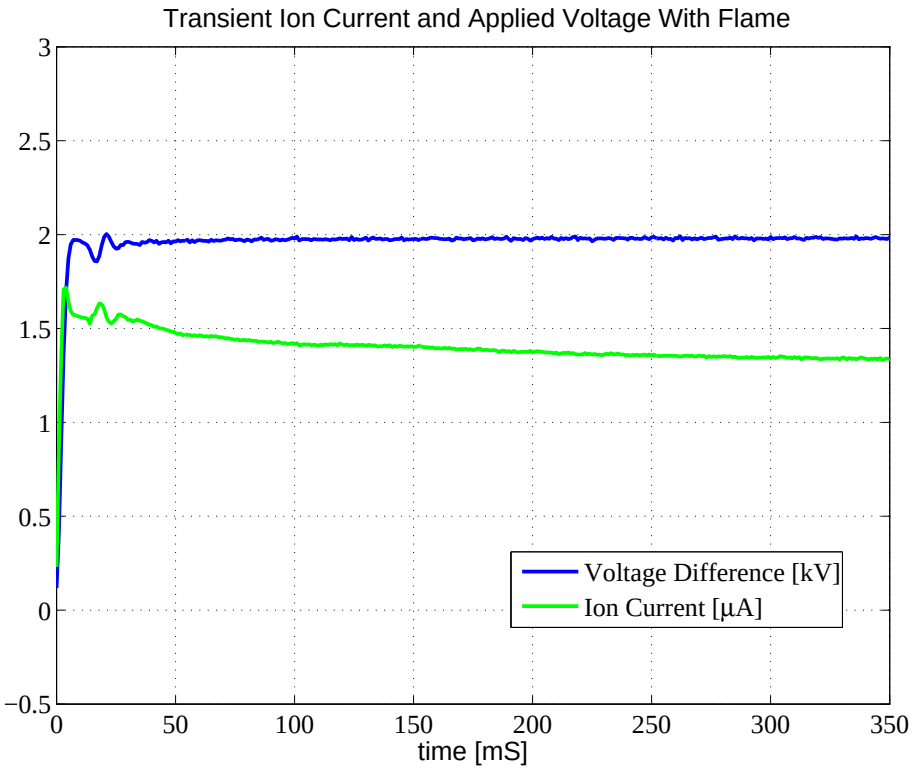

Figure 4.12: Transient voltage/current measurements corresponding with Fig. 4.11.

discussion. The two more popular beliefs were: (i) thermal ionization where an electron is released from its surface as the particle travels through the hot region of the flame or (ii) large ions are precursors to soot inception. Over the past 20 years (ii) has become less and less popular amongst the soot community due to increasing popularity in neutral polycyclic aromatic hydrocarbon (PAH) mechanisms based on free radicals, e.g., [8, 39].

The results in Fig. 4.11 and 4.12 also suggests that (ii) must not be true due to the fact that the residence time of ions within the flame is shortened due to the coulomb force directing the positive ions toward the burner. If (ii) were true then it would be reasonable to think that the visible appearance of soot would disappear on a time-scale similar to the generation of an ion current. The ion current measurement in Fig. 4.11 shows a current reading close to 1.5μA within 10ms. This means that even if an ion/electron sheath is surrounding the flame, a good percentage of the positive ions (if not all) are pulled out of the flame very

quickly. One of the strongest arguments against positive ions as precursors to soot has been that the concentration of ions in flames is too weak to account for the concentration of soot. Yet the soot region is still visible up to 40ms. This is evidence that positive ions are not a major chemical contributor to soot production. This conclusion agrees with the conclusions of [8, 39].

It is also interesting to note that the sooty region doesn't seem to be directly affected by the electric field at all. This means that if the soot particles are charged, either the electrons are sheathing them from the electric field or the coulomb force on the soot particles is small compared to forces due to drag or buoyancy. The other possibility is that they are not charged at all. However, this is not the case since, as stated before, the ion current measurement and visible soot appear to be directly linked.

An ion wind effect, not chemical, seems to explain the phenomena best. This slow decay in visible traces of soot must be due to an alteration in the temperature field within the combustion environment. The relationship between the decay in the visible appearance of soot and the decay in ion current in Fig. 4.12 can be explained by (i). That is, the electrohydrodynamics is slowly producing an environment opposed to soot production. As soot production decreases, less soot particles are available to release electrons via thermal ionization. However, this reasoning is not strongly conclusive and requires further investigation.

4.3.4 Negative to Positive Field

The time-scale analysis from Section. 4.2 was performed assuming the body forces due buoyancy and electric field are decoupled and the initial gas velocity near the exit of the tube is ≈0cm/s. The experiment in Fig. 4.13 tried to create this scenario by having the flame initially sitting in a negative electric field where the electrical body force in the flame region is acting against the exiting gas from the fuel tube. This reduces the gas velocity

near the flame. At t=0ms, the polarity of the electric field is switched to a positive field as can be seen in Fig. 4.14. While the applied voltage is seen to be slow reacting (≈60ms), the ion-current is shown to become established relatively quickly (≈10ms).

The initial thermal plume profile before the electric field polarity switch is very similar to the final profile seen in Fig. 4.9(c). That is, the lower portion of the thermal plume profile is round and wide compared to the thinner upper portion of the plume. The first noticeable motion in the thermal plume occurs at ≈10ms after the polarity switch. The motion resembles the motion seen in Fig. 4.5. The base of the plume rises and a wave front in the plume is set into motion downstream. The most noticeable difference between Figs. 4.5 and 4.13 is the intensity of this motion. In Figs. 4.13(c) and (d), the base of the plume is lifted past the height of the fuel tube exit for a brief moment before reattaching itself to the tube. When considering the strength of the ion wind is expected to be on the same order of magnitude as the case of a 0 to positive field step, this lifted thermal plume is an unexpected result. Analyzing this lifted thermal plume becomes complex and will then be interpreted in parallel with the flame video in the upcoming paragraphs. Two secondary waves are seen to form as can be seen in Fig. 4.13(f) and (i). The overall time it takes the thermal plume to reach a new steady state is ≈144ms. The initial plume travels at an average speed ≈60cm/s. This is three quarters slower than the wave velocity of the 0 to positive field step function (section 4.3.2). It is easy to attribute this to the slower rising time of the HV power supplies. However, once again the ion current measurement indicates an established positive ion flux through the electrode gap relatively quickly. Thus, the answer must be the ion flux itself. The current measurement in Fig. 4.14 shows an unstable measurement when compared to Fig. 4.6. Once the ion current's polarity changes, the ion current struggles to reach the steady state value of 2μA. One explanation is that in the initial state, electrons are traveling toward the downstream electrode while the positive ions neutralize at the burner. When the polarity of the electric field is switched, the direction of ions and electrons are also reversed. The two oppositely charged clouds must cross paths and in doing so may recombine with

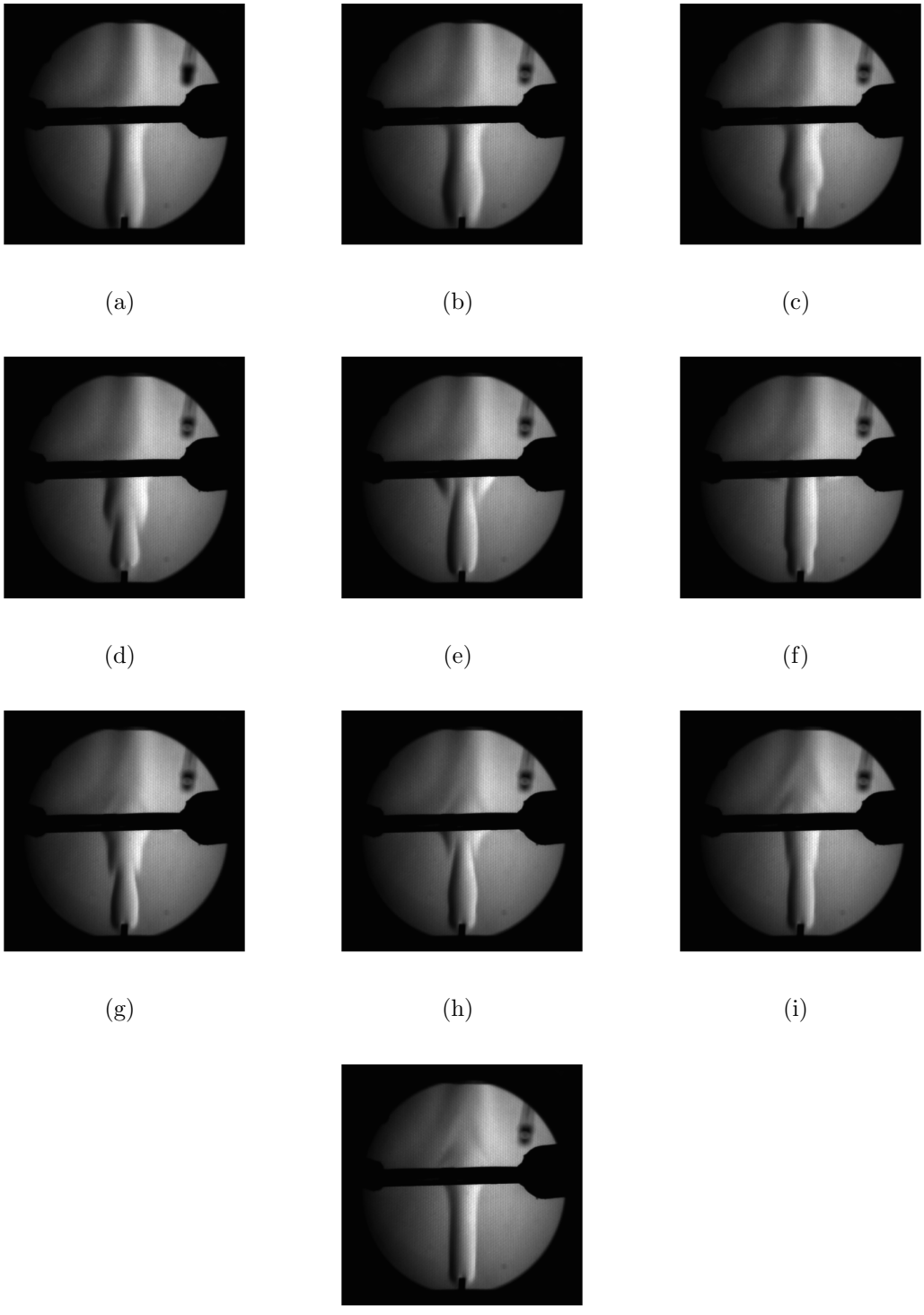

(a) (b) (c)

(d) (e) (f)

(g) (h) (i)

(j)

Figure 4.13: Snapshots taken from high-speed video of the methane flame (negative to positive field): (a) t<0ms, (b) 21ms, (c) 33ms, (d) 46ms, (e) 60ms, (f) 72ms, (g) 86ms, (h) 94ms, (i) 114ms, (j) 144ms,.

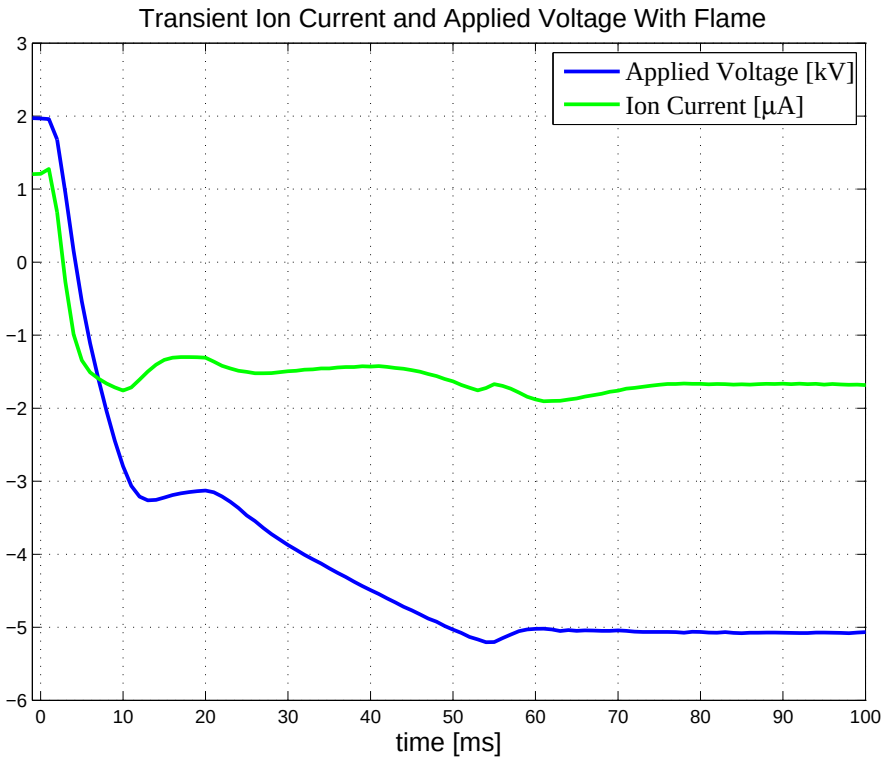

Figure 4.14: Transient voltage/current measurements corresponding with Fig. 4.13.

each other. This occurrence would reduce the ion wind effect. Another possibility is that since the bulk gas has a slower initial velocity, more ion/neutral collisions are required in order to create the same effect that was seen in section 4.3.2. However, this is unlikely. Xu [42] calculated that the number of ion/neutral collisions required to transfer 99.9% of the ion's kinetic energy acquired by an electric field to the neutral gas flow is on the order of tens of collisions. This is a very small effect and should contribute very small variations to the gas flow.

Images from the flame video are shown in Fig. 4.15 and the corresponding transient voltage and ion current measurements in Fig. 4.16. The first still image, Fig. 4.15(a), shows the flame in its initial steady state. This is the same state as described in Fig. 4.13(a).

As the polarity of the field is switched at t_o=0ms, the flame is seen to lift off the burner tip, Figs. 4.15(b)-(d). What causes the flame to lift is again the positive ions, (originally

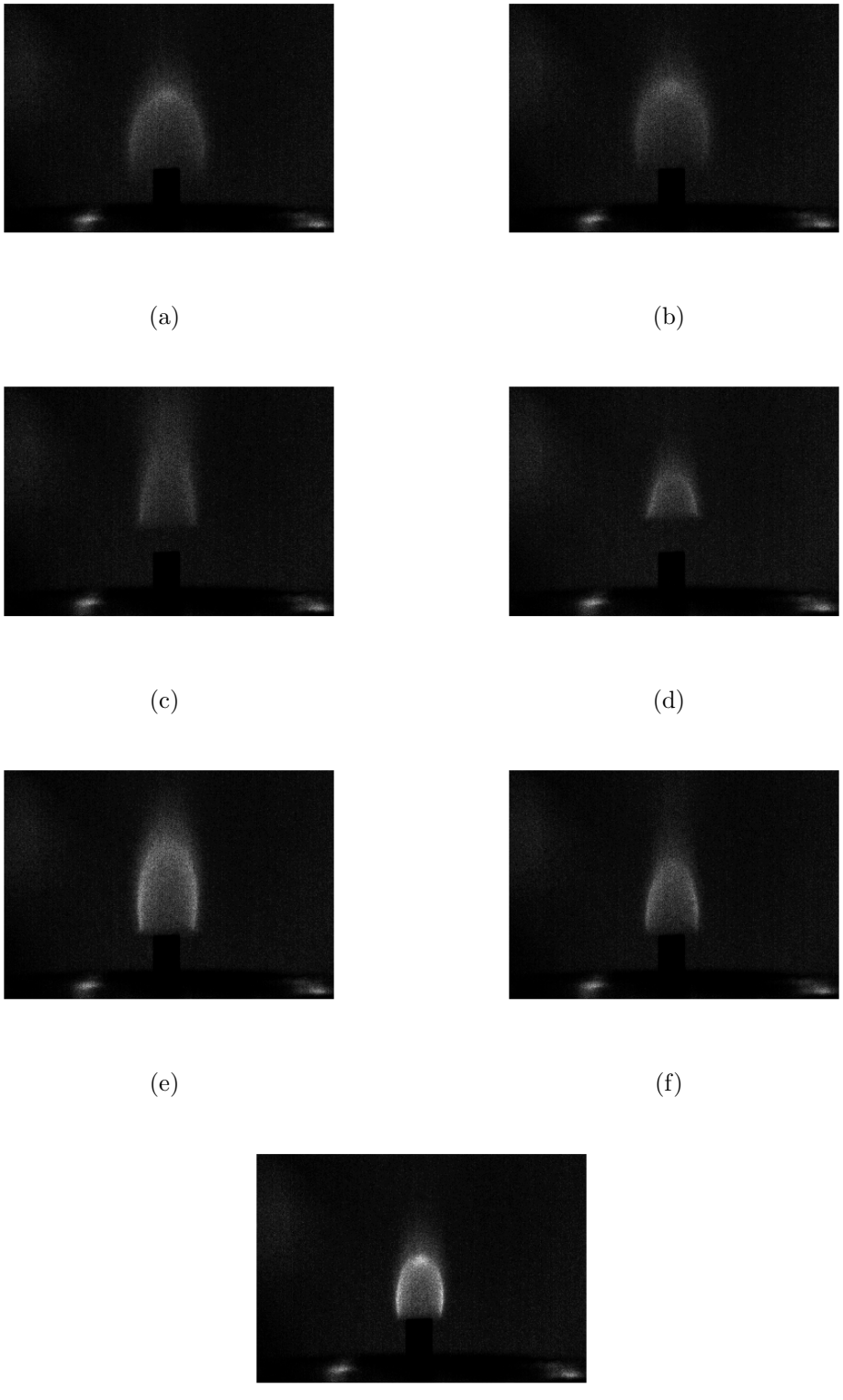

(a) (b) (c) (d) (e) (f) (g)

Figure 4.15: Snapshots taken from high-speed flame video (negative to positive field): (a) t>0ms, (b) 10ms, (c) 15ms, (d) 19ms, (e) 26ms, (f) 31ms, (g) 46ms.

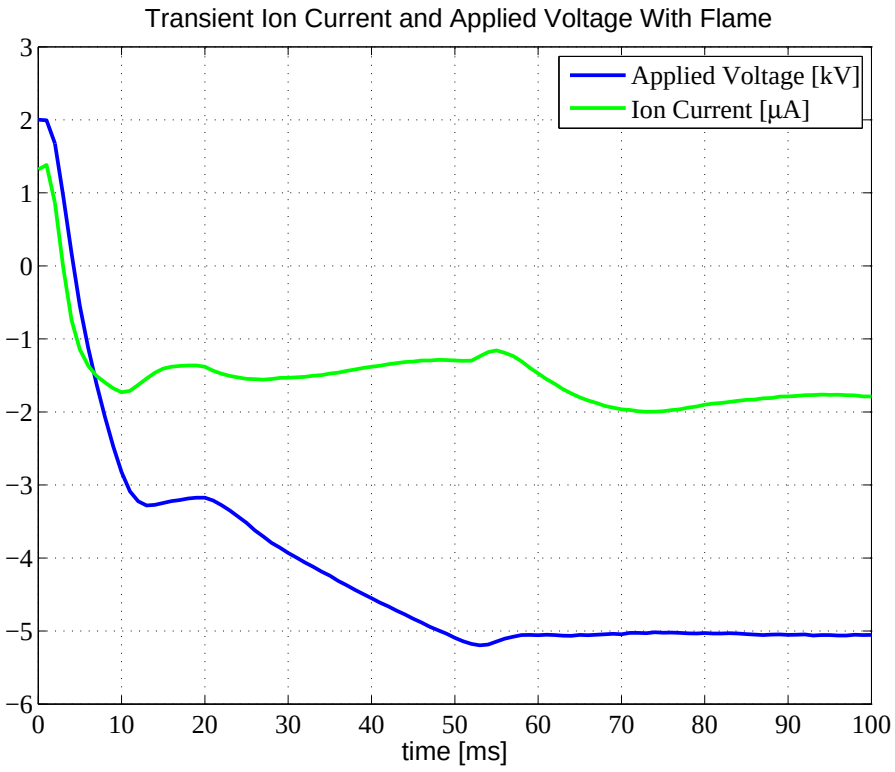

Figure 4.16: Transient voltage/current measurements corresponding with Fig. 4.15.

pulled towards the burner) being redirected downstream. This creates a mechanical drag effect in the bulk fluid that is more intense than what was seen in Fig. 4.7. This most likely due to the fact that the initial bulk gas velocity in the region close to the flame is slower than the 0 to positive field step case. Therefore, the frequency of collisions between ions and neutral molecules is higher and the ion wind is able to generate faster. The axial velocity increases faster and the flame lifts off the burner and nearly becomes extinguished. This is proceeded by an entrainment of cool ambient air that floods the region below the lifted flame as can be seen in the schlieren images, e.g. Fig. 4.13(d). The air mixes with the fuel creating a premixed gas. Eventually the combustion reaction is able to catch up and the flame re-attaches to the burner tip, Figs. 4.15(d)-(f). After the re-attachment, The flame shape shrinks and increases in luminosity. The final flame shape is seen in Fig. 4.15(g).

Chapter 5

Summary and Conclusion

The experiments described in this thesis used a schlieren system to visualize the motion of hot exhaust gases from a methane flame placed in between two electrodes. A high speed camera was to used to capture this motion as the electric potential between the two electrodes went through various step changes; a zero to positive saturation field, a zero to negative saturation field, and a negative to positive saturation field. The videos show dramatic changes in the shape of the thermal plume in all three cases.

The video containing the positive electric field showed a never before seen wave like motion in the thermal plume starting at the flame base and propagating toward the downstream electrode. This thermal plume wave was explained to be caused by an ion driven wind acting on the hot gases. The average velocity of the wave ($L/\triangle t$) was measured to be ≈80cm/s. This was compared to theoretical average and maximum velocities which were calculated to be 124cm/s and 187cm/s, respectively. The final plume boundary was seen to be thinner than the case with no field. The final plume form was achieved ≈90ms after the electric field was initiated. The establishment of an ion wind appeared to occur very fast ($< 10ms$) after the establishment of an ion flux.

The video containing the negative electric field showed a much different result. The position of the thermal plume dropped closer to the burner. The final shape of the plume resembled similar to an upside down incandescent light bulb; the bottom portion of plume boundary much thicker than the top. This effect was also described by an ion driven wind. The final plume shape was also achieved ≈90ms after the electric field was initiated.

The video containing the negative to positive electric field transition showed a similar wave propagation in the thermal plume similar to the video in the zero to positive field. However, this wave was much more intense near the flame, so much so that the thermal plume was able to completely lift off the burner tip momentarily before reattaching to the burner. The separation of the flame from the burner was attributed to the increasing axial velocity due to an ion wind followed by entrainment of cool ambient air mixing into the region just above the burner fuel tube. The average velocity of the thermal plume wave was measured to be ≈60cm/s. The final plume form was achieved after ≈144ms after the electric field polarity switch was initiated.

In all three cases, transient electrode potentials were generated much slower than ideal situation. This was shown to be due to the slow capacitance charging capabilities of the high voltage power supply system. A future study using a faster high voltage power supply is still needed to confirm that this is not affecting the other measured time-scales. However, saturation ion current measurements were achieved within 8-10ms after electric field step was initiated. This is evidence that an ion flux has become established within the gas. This ion current time-scale matched well with the time-scale related to the initiation of the hydrodynamic effect seen in the schlieren videos. It should be noted that the ion current 8-10ms rise time is slower than predicted by theory. This may be due to the flame ions acting as a ion sheath to the electric field. Further investigation is needed to understand this.

High-speed videos of the flame were also taken to complement the schlieren videos. In all three cases, the flame went through significant changes. The changes were seen to initiate

≈8-10ms after the change in electric field was initiated in all three cases. The flame shape arrived at a new steady state after ≈40ms. The significance of this value is that even after the flame has stabilized, much is still occurring downstream of the flame. In fact, the steady state of the entire system is reached more than twice the time of the flame reaching steady state. A positive field produced a final shape that was shorter, thinner, more luminous, and almost entirely soot free when compared to the flame without an electric field. A negative field produced a final shape that was much wider, less luminous, and soot free. However, a gradual decay in the sooty region of the flame occurred with a negative field that matched very well with the decay in measured ion current. This decay lasted ≈320ms. This differed from the positive field case which saw the disappearance of its sooty region with a time-scale on the same order as the flame stabilization time-scale. The relationship between flame chemi-ions and soot has been previously published in the literature. However, this strong connection between appearance of soot and measured ion current has never been seen before. It was hypothesized, not concluded, that the disappearance of the sooty region of the flame with a negative field was due to a change in the temperature field. Finally, the negative field experiment provides evidence that soot particles are a source for charged species by means of thermal ionization and that positive ions are not precursors to soot.

Chapter 6

Future Work

Much research from the literature on electric field effects on flame dynamics have mostly focused on steady-state problems. Transient studies provide clues to questions that cannot be solved by steady-state and AC field studies. As far as this author is aware of, the transient effects presented in this thesis show phenomena never before seen for an axisymmetric methane flame. This chapter discusses future experiments that need to be performed to answer questions that are still left unanswered.

This thesis mainly emphasized a way to solve time-scale problems. The time-scales described consisted of the following,

A) initiation of an electric field

B) development of an ion current

C) initiation of an ion wind

D) stabilization of hydrodynamics

E) stabilization of combustion

F) decay in the appearance of soot

Most items seemed to match theoretical time-scales within reason. However, item B is still up for question. This was explained in previous chapters to be due to the slow capacitance charging capability of the high voltage power supply producing a gradually increasing charge on the electrodes. A fast charging high voltage power supply is needed to confirm that this is not affecting the ion current time-scale. If this time-scale is seen to be different with such a HV power supply, the other time-scales are more than likely to be affected.

Other than time scales, other parameters that need to be studied include fuel flow rate, length scales, and field strength. These parameters are needed for a higher understanding of which applications are actually practical for flame ions. For instance, does it make sense to use a chemi-ion producing fuel if a plasma generated by corona discharge is more beneficial. What system scales makes sense to utilize an electric field to assist combustion, e.g. large power generation plants or small handheld burners? These scaling parameters will be studied in the future with emphasis on transient affects.

It was mentioned earlier in this thesis that the ion current rise time was slower than expected by almost an order of magnitude. This was explained to be due to flame ions acting as a shield against the electric field. A future study will be performed using a Langmuir probe to study how the flame ions affect the space charge within the electrode space. A Langmuir probe may also provide a way to determine the current density profile of the ion stream. This will provide a way to quantify the electrical body force acting on the mostly neutral gas and to predict the ion wind driven gas velocities.

Ideally, PIV could provide a more quantitative method for measuring velocity fields within the electrode space. However, a thorough investigation on particle charging is needed to ensure the reliable results. More specifically, if the injection of particles into the gas stream is seen to effect schlieren boundaries and/or voltage current curves, then PIV certainly is

not a trustworthy method for measuring gas velocities in a combustion system subjected to an electric field.

Methods for measuring the temperature field of a gas within an electric field has been a difficult task since the very nature of the electric field does not allow for accurate measurements with probes. Laser diagnostic techniques, such as Rayleigh scattering thermometry, may provide a means to acquiring reliable measurements. This would be especially useful in studying the transient soot effects shown Chapter 4.

Computer simulations that include a reduced ion chemistry still needs to be developed in order to test the conclusions of these experiments. As discussed previously, computer simulations remain a very difficult task, even for one dimensional problems.

Finally, as stated consistently throughout this thesis, experiments performed in a gravity-less environment is absolutely essential for separating the effects created by buoyancy from those created by the ion wind. Experiments on-board the ISS and on the NASA Glenn drop-tower would create a suitable environment for this decoupling.

Bibliography

[1] F. Borgatelli and D. Dunn-Rankin. Behavior of a small diffusion flame as an electrically active component in a high-voltage circuit. *Combustion and Flame*, 159(1):210–220, Jan. 2012.

[2] R. Bowser and F. Weinberg. The effect of direct electric fields on normal burning velocity. *Combustion and Flame*, 18(2):296–300, Apr. 1972.

[3] H. Calcote. Ion and electron profiles in flames. *Symposium (International) on Combustion*, 1963.

[4] H. F. Calcote. Electrical properties of flames. *Symposium on Combustion and Flame, and Explosion Phenomena*, 3(1):245–253, 1948.

[5] F. Carleton and F. Weinberg. Electric field-induced flame convection in the absence of gravity. *Nature*, 1987.

[6] D. Dunn-Rankin and F. J. Weinberg. Using large electric fields to control transport in microgravity. *Annals of the New York Academy of Sciences*, 1077:570–84, Sept. 2006.

[7] A. Fialkov. Investigations on ions in flames. *Progress in Energy and Combustion Science*, 23:399–528, 1997.

[8] a. B. Fialkov, a. N. Hayhurst, S. G. Taylor, and S. B. Newcomb. Shapes of Soot Particles, Both Charged and Uncharged, after Molecular Beam Sampling a Premixed Oxyacetylene Flame, Burning at Atmospheric Pressure. *Combustion Science and Technology*, 185(12):1762–1776, Dec. 2013.

[9] T. Fujii. Theory of the steady laminar natural convectiol above a horizontal line heat source and a point heat source. *International Journal of Heat and Mass Transfer*, 6(6):597–606, 1963.

[10] J. Goodings, D. Bohme, and C.-W. Ng. Detailed ion chemistry in methane-oxygen flames. I. Positive ions. *Combustion and Flame*, 36:27–43, Jan. 1979.

[11] J. Goodings, D. Bohme, and C.-W. Ng. Detailed ion chemistry in methane-oxygen flames. II. Negative ions. *Combustion and Flame*, 36:45–62, Jan. 1979.

[12] J. Green and T. Sugden. Some observations on the mechanism of ionization in flames containing hydrocarbons. *Symposium (International) on Combustion*, 9(1):607–621, Jan. 1963.

[13] K. Gugan, J. Lawton, and F. Weinberg. The response of droplets and particles to electric fields, in the presence of ions. *Symposium (International) on Combustion*, 10(1):709–720, Jan. 1965.

[14] R. Heinsohn, S. Thillard, and P. Becker. Temperature profiles of an opposed-jet diffusion flame subjected to an electric field. *Combustion and Flame*, pages 442–445, 1969.

[15] R. Heinsohn, D. Wulfhorst, and P. Becker. The effects of an electric field on an opposed-jet diffusion flame. *Combustion and Flame*, 1967.

[16] H. Jaggers and A. V. Engel. The effect of electric fields on the burning velocity of various flames. *Combustion and Flame*, 285, 1971.

[17] S. Karnani. *Electric field-driven flame dynamics*. PhD thesis, Irvine, Calif. :, 2011.

[18] S. Karnani. *Electric Field-Driven Flame Dynamics*. 2012.

[19] S. Karnani, D. Dunn-Rankin, F. Takahashi, Z.-G. Yuan, and D. Stocker. Simulating Gravity in Microgravity Combustion Using Electric Fields. *Combustion Science and Technology*, 184(10-11):1891–1902, Oct. 2012.

[20] M. Kono, F. Carleton, A. Jones, and F. Weinberg. The effect of nonsteady electric fields on sooting flames. *Combustion and flame*, 4:357–364, 1989.

[21] M. Kono, K. IInuma, and S. Kumagai. The effect of dc to 10 MHz electric field on flame luminosity and carbon formation. *Symposium (International) on Combustion*, 18(1):1167–1174, Jan. 1981.

[22] J. Kuhl, G. Jovicic, L. Zigan, and A. Leipertz. Transient electric field response of laminar premixed flames. *Proceedings of the Combustion Institute*, 34(2):3303–3310, Jan. 2013.

[23] J. Lawton, P. J. Mayo, and F. J. Weinberg. Electrical Control of Gas Flows in Combustion Processes. *Proceedings of the Royal Society A: Mathematical, Physical and Engineering Sciences*, 303(1474):275–298, Mar. 1968.

[24] J. Lawton and F. J. Weinberg. Maximum Ion Currents from Flames and the Maximum Practical Effects of Applied Electric Fields. *Proceedings of the Royal Society A: Mathematical, Physical and Engineering Sciences*, 277(1371):468–497, Feb. 1964.

[25] J. Lawton and F. J. Weinberg. *Electrical Aspects of Combustion*. Oxford University Press, 1970.

[26] P. J. Mayo and F. J. Weinberg. On the Size, Charge and Number-Rate of Formation of Carbon Particles in Flames Subjected to Electric Fields. *Proceedings of the Royal Society A: Mathematical, Physical and Engineering Sciences*, 319(1538):351–371, Oct. 1970.

[27] W. Miller. Ions in flames: evaluation and prognosis. *Symposium (International) on Combustion*, 1973.

[28] M. J. Papac and D. Dunn-Rankin. Canceling buoyancy of gaseous fuel flames in a gravitational environment using an ion-driven wind. *Annals of the New York Academy of Sciences*, 1077:585–601, Sept. 2006.

[29] M. J. Papac and D. Dunn-Rankin. Modelling electric field driven convection in small combustion plasmas and surrounding gases. *Combustion Theory and Modelling*, 12(1):23–44, Dec. 2007.

[30] T. Pedersen and R. C. Brown. Simulation of electric field effects in premixed methane flames. *Combustion and Flame*, 94(4):433–448, Sept. 1993.

[31] E. R. Place and F. J. Weinberg. Electrical Control of Flame Carbon. *Proceedings of the Royal Society A: Mathematical, Physical and Engineering Sciences*, 289(1417):192–205, Jan. 1966.

[32] J. Prager, U. Riedel, and J. Warnatz. Modeling ion chemistry and charged species diffusion in lean methane–oxygen flames. *Proceedings of the Combustion Institute*, 31(1):1129–1137, Jan. 2007.

[33] M. Rickard, D. Dunn-Rankin, F. Weinberg, and F. Carleton. Characterization of ionic wind velocity. *Journal of Electrostatics*, 63(6-10):711–716, June 2005.

[34] G. Settles. *Schlieren and Shadowgraph Techniques: Visualizing Phenomena in Transparent Media (Experimental Fluid Mechanics)*. Springer, 2001.

[35] A. Starik and N. Titova. Kinetics of ion formation in the volumetric reaction of methane with air. *Combustion, Explosion and Shock Waves*, 38(3):253–268, 2002.

[36] T. Sugden. Elementary combustion reactions. Charged species. *Symposium (International) on Combustion*, 1965.

[37] C. Vinckier, M. Gardner, and K. Bayes. A study of some primary and secondary chemi-ionization reactions in hydrocarbon oxidations. *Symposium (International) on Combustion*, 16(1):881–889, 1977.

[38] J. Vinogradov, E. Sher, I. Rutkevich, and M. Mond. Voltage-current characteristics of a flame-assisted unipolar corona. *Combustion and flame*, 2180(Vcc), 2001.

[39] H. Wang, B. Weiner, and M. Frenklach. Theoretical study of reaction between phenylvinyleum ion and acetylene. *The Journal of Physical ...*, pages 10364–10371, 1993.

[40] F. Weinberg, D. Dunn-Rankin, F. Carleton, S. Karnani, C. Markides, and M. Zhai. Electrical aspects of flame quenching. *Proceedings of the Combustion Institute*, 34(2):3295–3301, Jan. 2013.

[41] F. J. Weinberg. *Optics of Flames: Including Methods for the Study of Refractive Index Fields in Combustion and Aerodynamics*. Butterworths, 1963.

[42] K. G. Xu. Plasma sheath behavior and ionic wind effect in electric field modified flames. *Combustion and Flame*, Dec. 2013.

Appendices

A Transient Ion Current Measurements

The following plots show transient ion current measurements in response to different voltage step function commands. These tests were performed at different electrode spacings; 20-35mm gaps. Figures A.1 & A.2 show the measurements for a 20 mm gap. In Figure A.1(e) & (f), an instability occurs in the measurement and is seen as a 75HZ oscillation. In Figures A.3 & A.4 (25mm spacing), the oscillation is also present but with a smaller peak to peak value. In Figures A.5 & A.6 (30mm spacing), the oscillation is hardly noticable. In Figures A.7 & A.8 (35mm spacing), no oscillation can be seen.

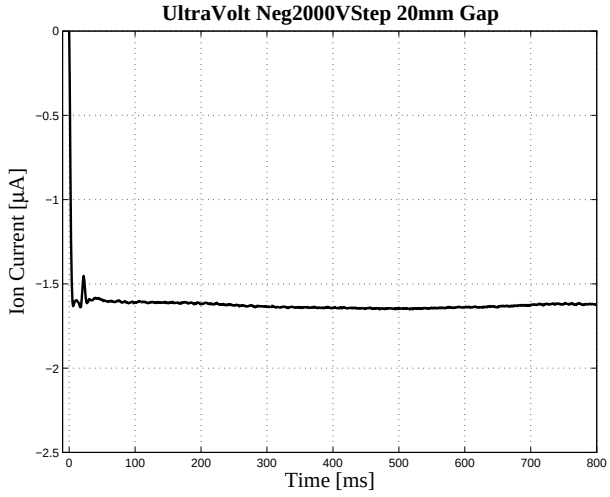

(a) -2kV

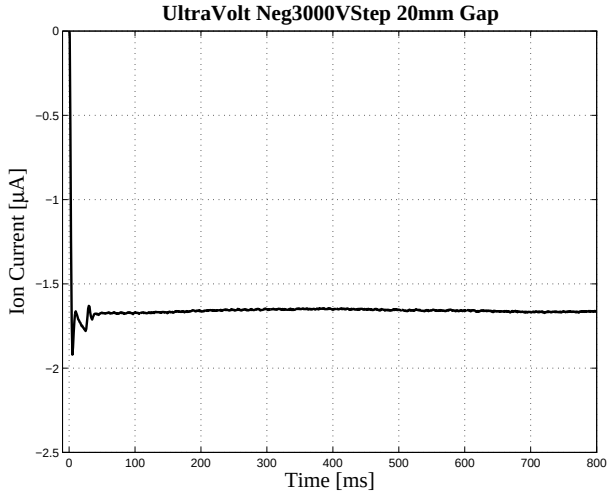

(b) -3kV

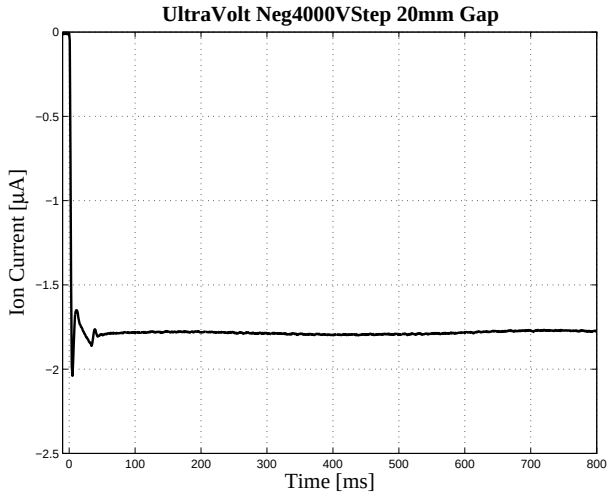

(c) -4kV

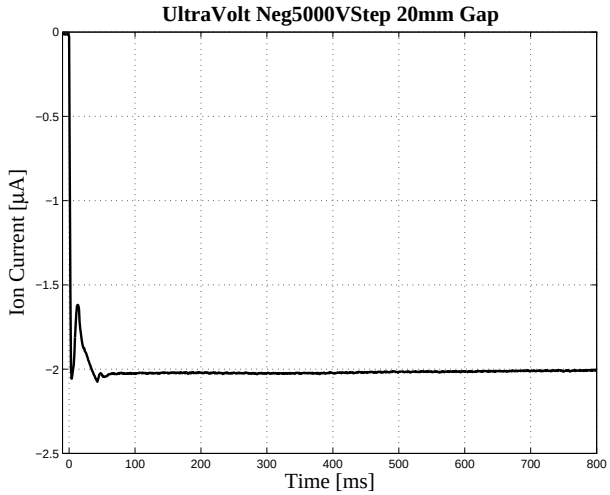

(d) -5kV

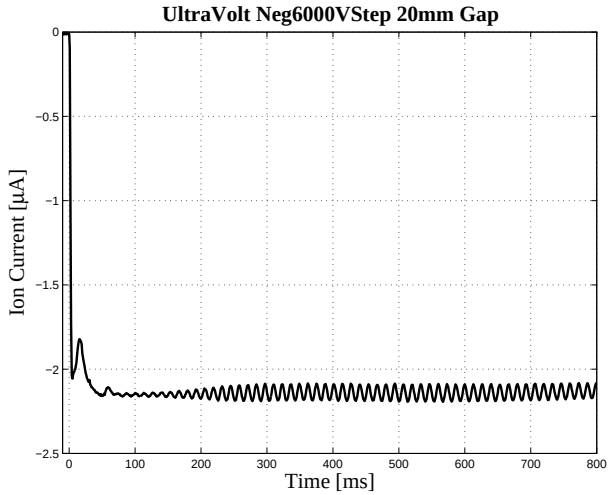

(e) -6kV

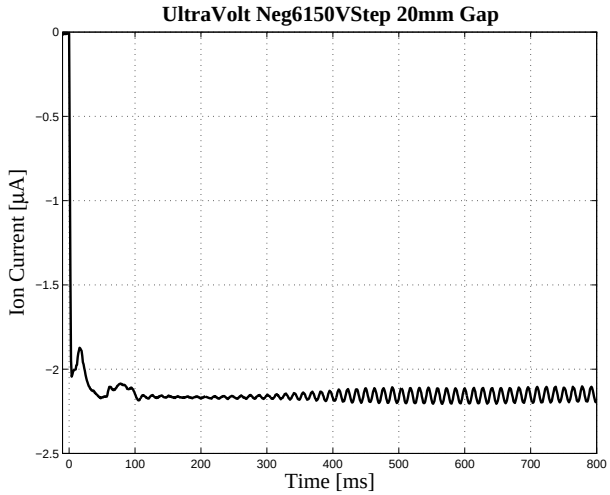

(f) -6.15kV

Figure A.1: Ion Current Measurements - 20mm electrode spacing

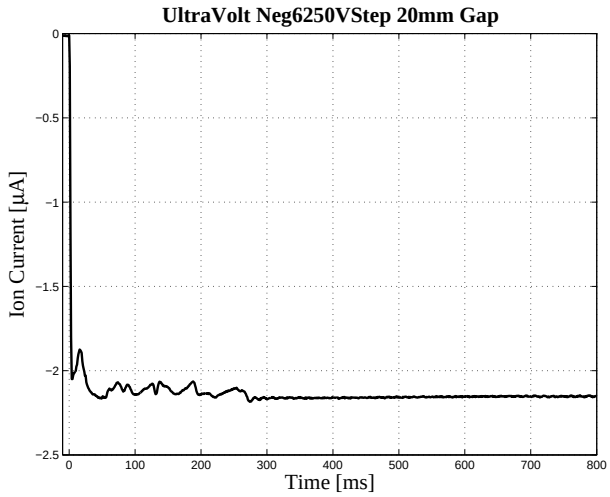

(a) -6.25kV

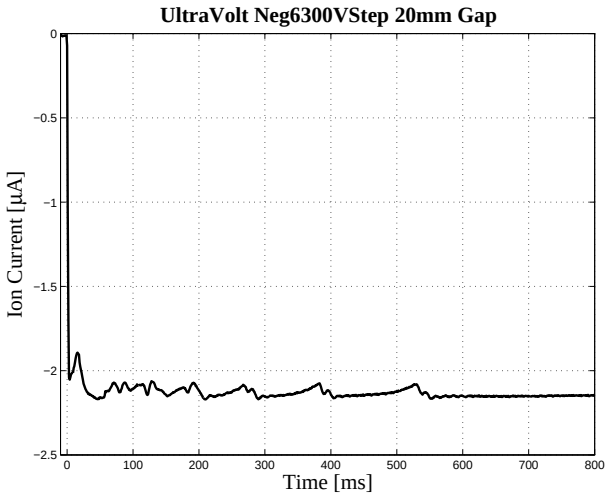

(b) -6.3kV

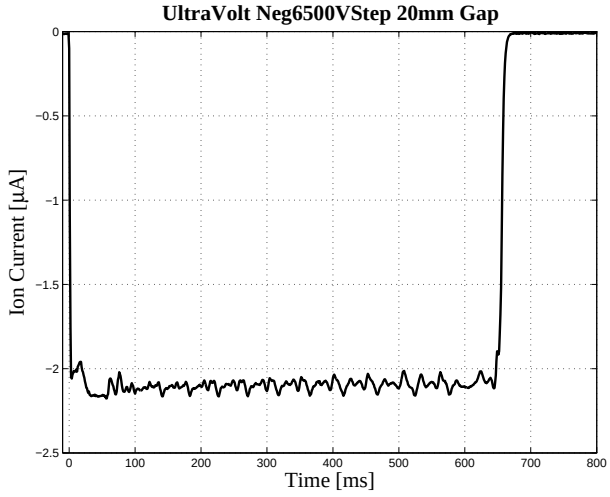

(c) -6.5kV

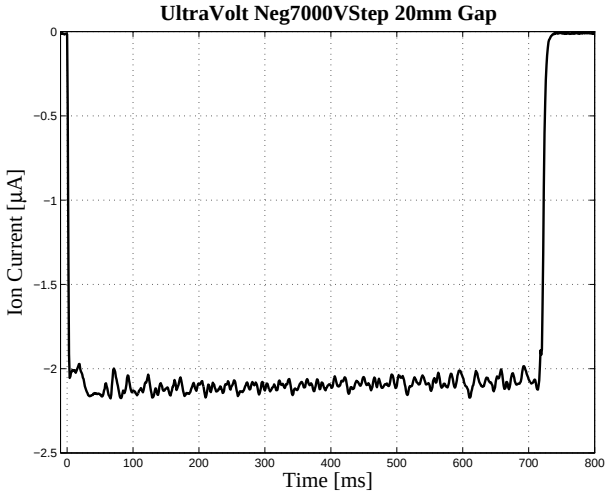

(d) -7kV

Figure A.2: Ion Current Measurements - 20mm electrode spacing continued

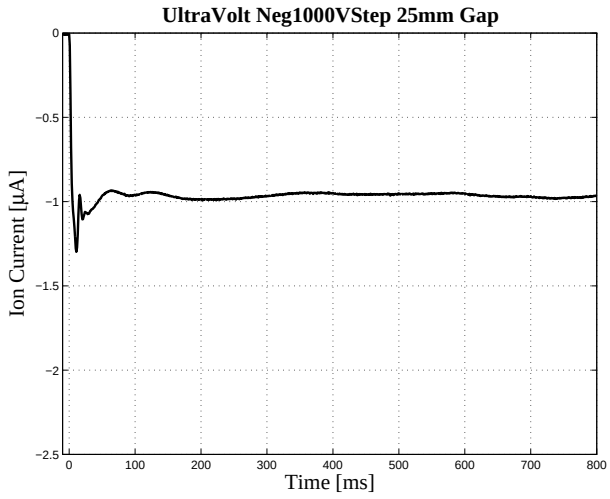

(a) -1kV

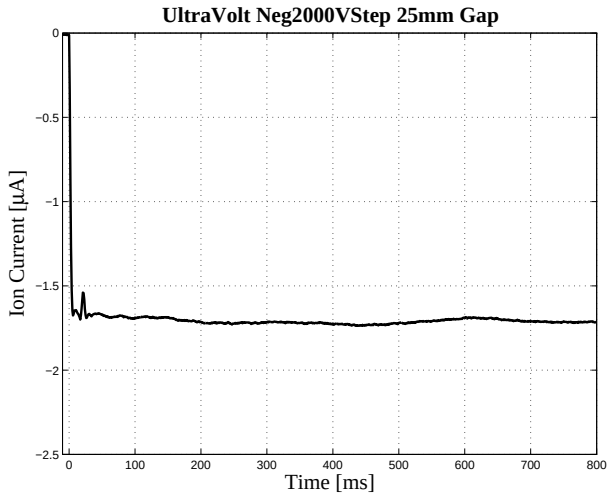

(b) -2kV

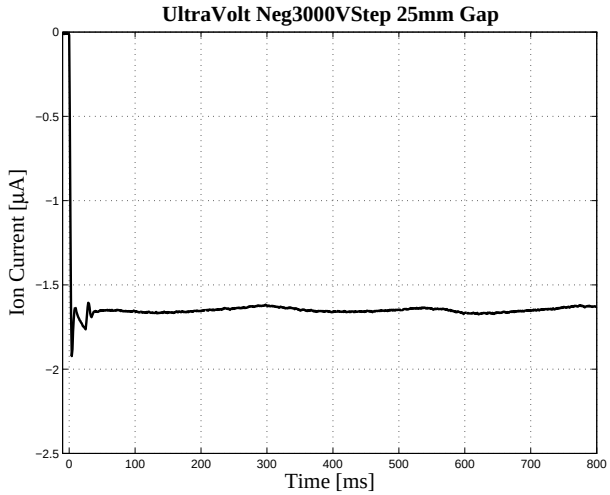

(c) -3kV

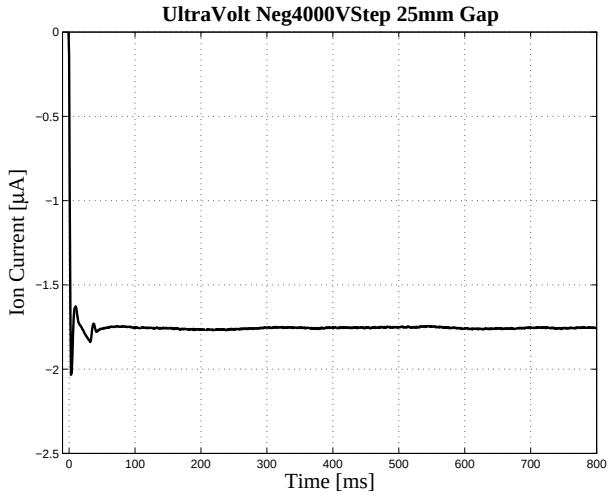

(d) -4kV

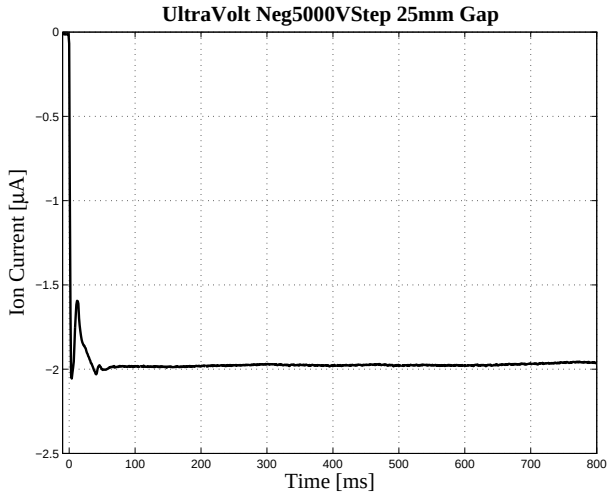

(e) -5kV

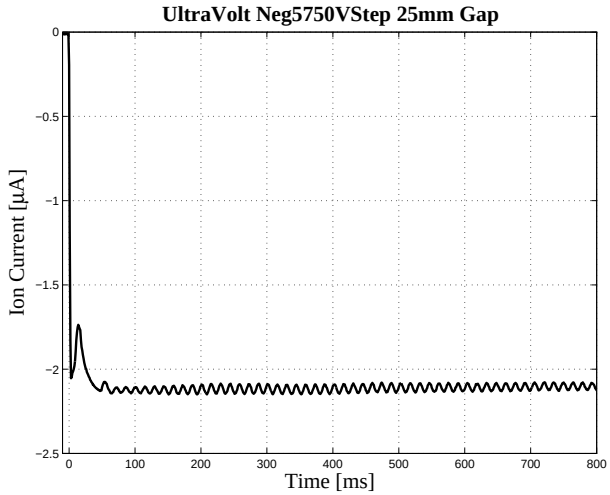

(f) -5.75kV

Figure A.3: Ion Current Measurements - 25mm electrode spacing

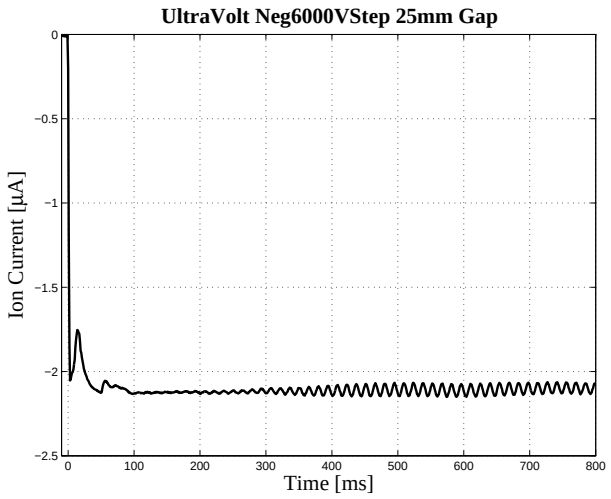

(a) -6kV

Figure A.4: Ion Current Measurements - 25mm electrode spacing continued

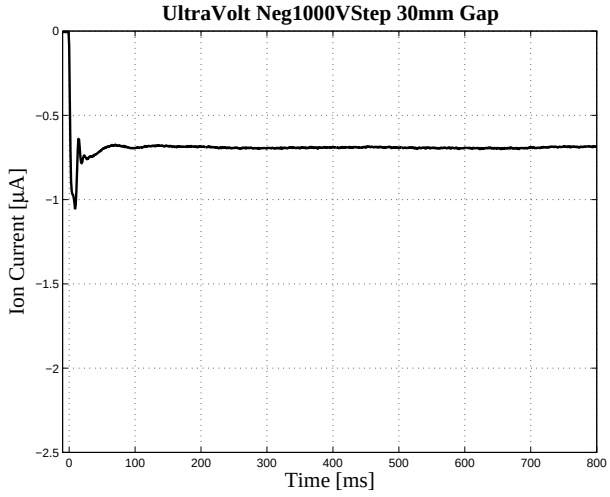

(a) -1kV

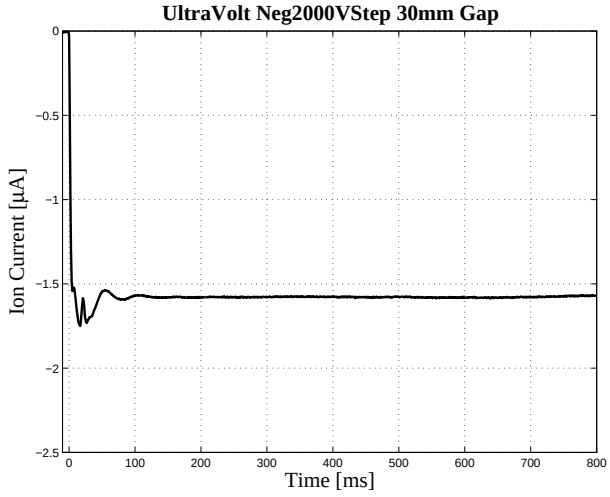

(b) -2kV

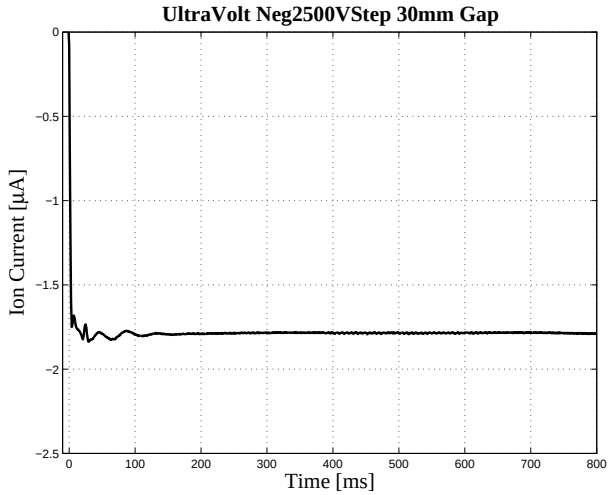

(c) -2.5kV

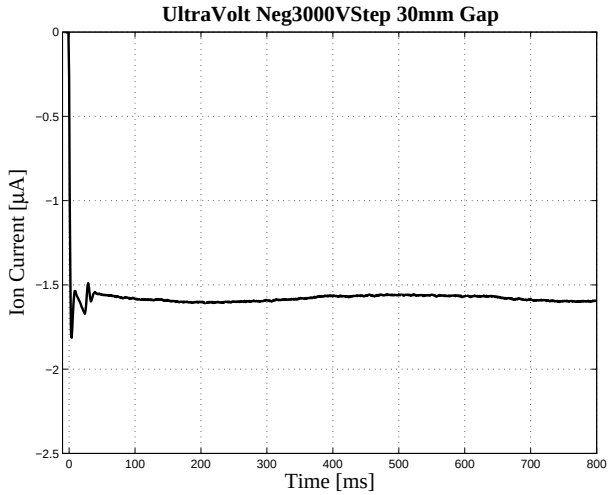

(d) -3kV

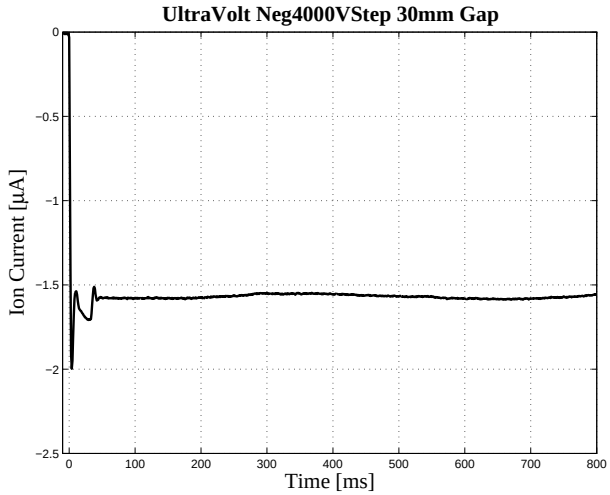

(e) -4kV

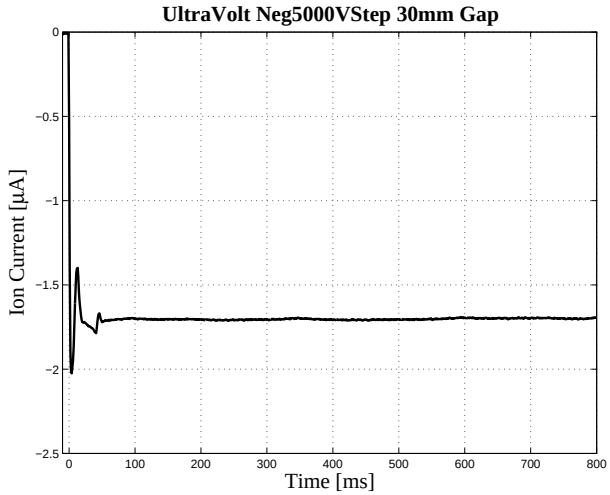

(f) -5kV

Figure A.5: Ion Current Measurements - 30mm electrode spacing

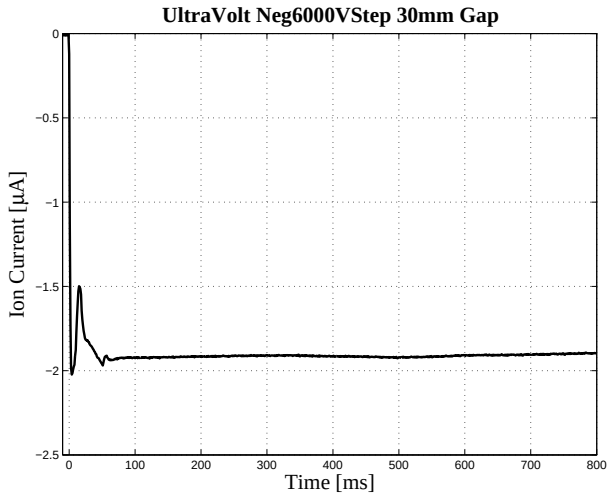

(a) -6kV

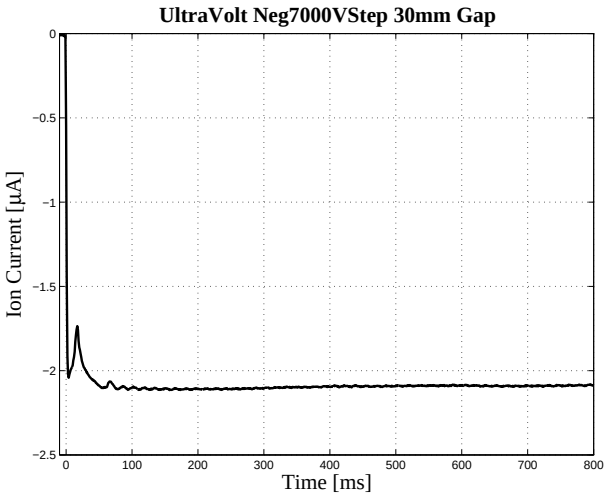

(b) -7kV

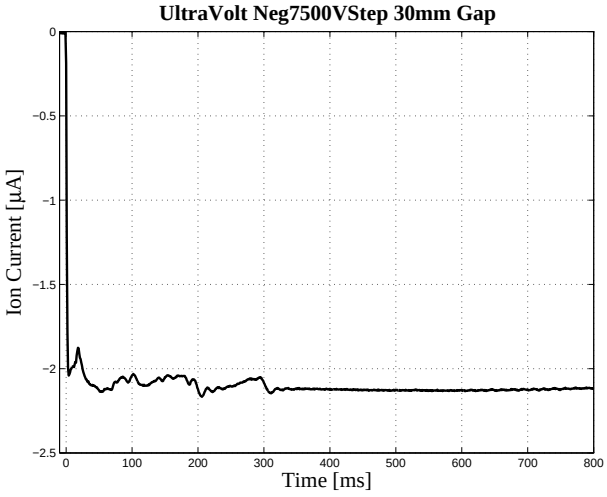

(c) -7.5kV

Figure A.6: Ion Current Measurements - 30mm electrode spacing continued

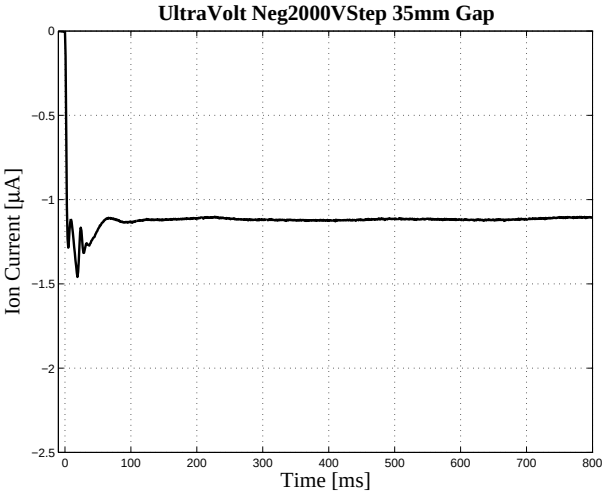

(a) -2kV

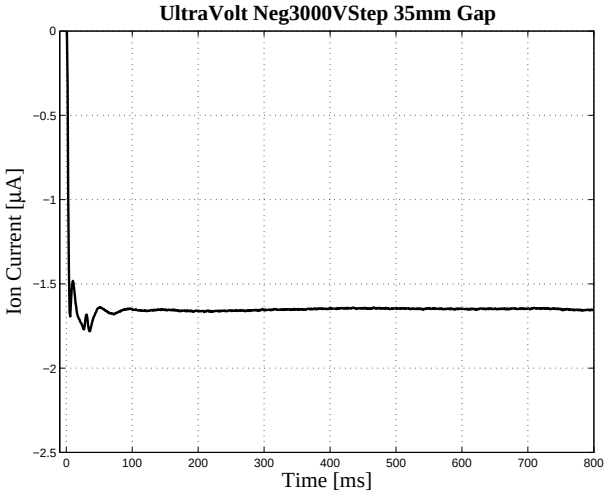

(b) -3kV

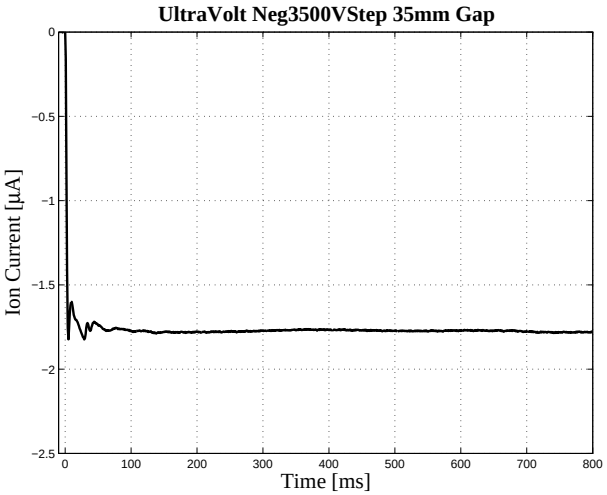

(c) -3.5kV

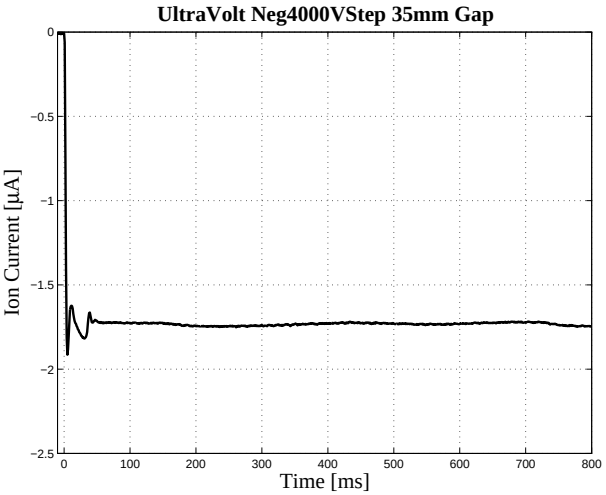

(d) -4kV

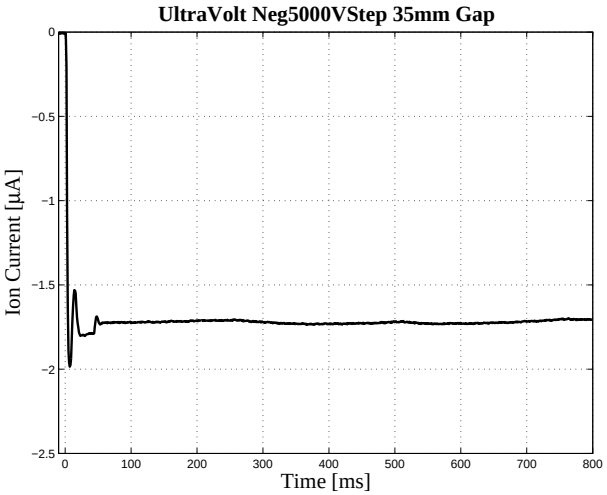

(e) -5kV

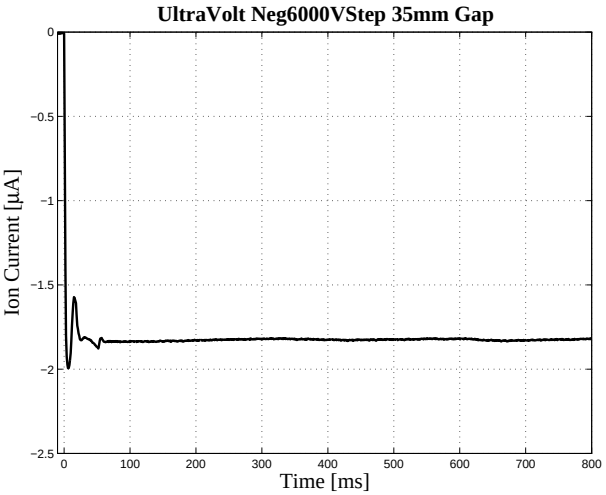

(f) -6kV

Figure A.7: Ion Current Measurements - 35mm electrode spacing

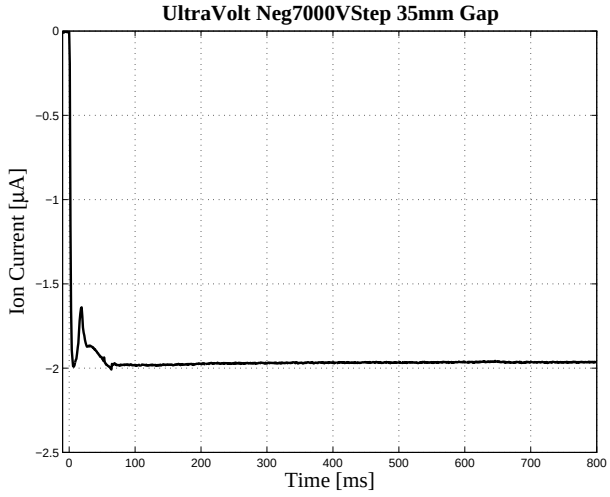

(a) -7kV

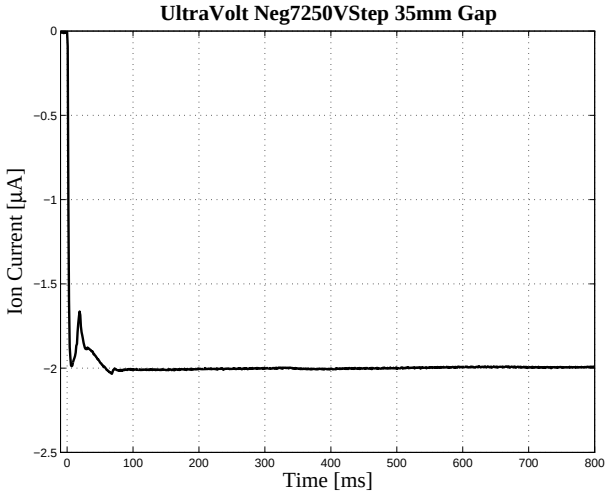

(b) -7.25kV

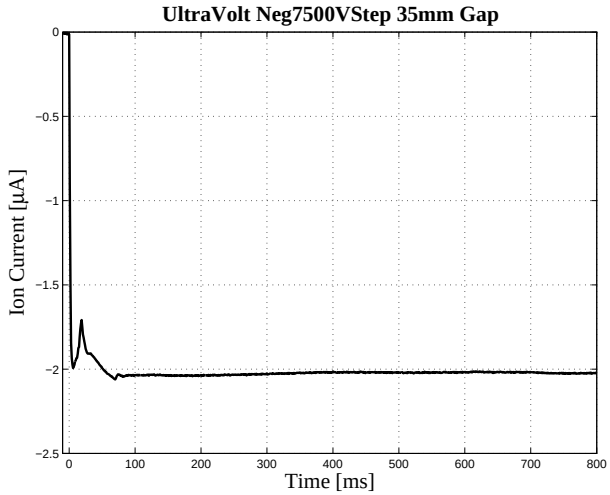

(c) -7.5kV

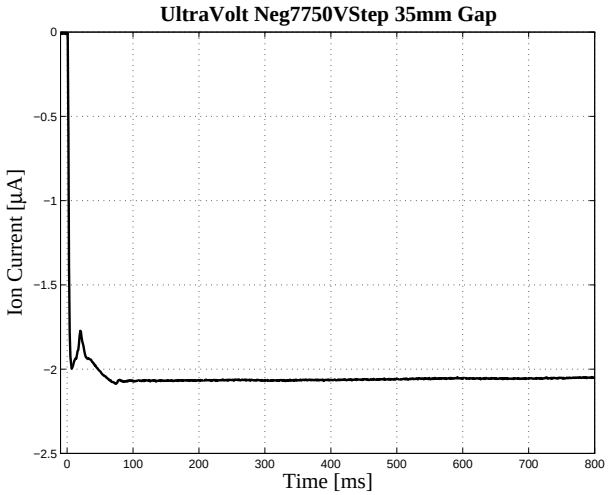

(d) -7.75kV

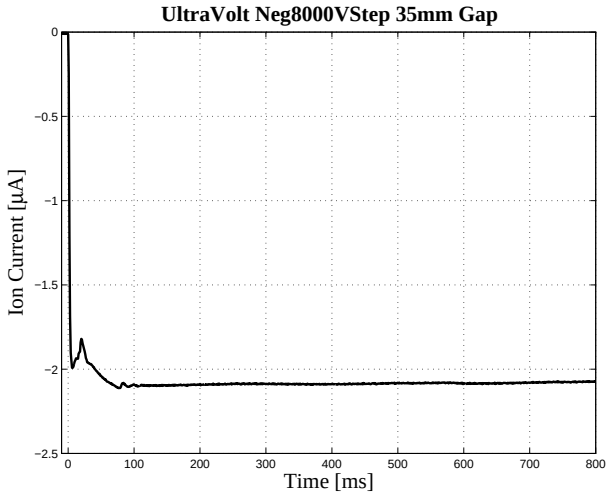

(e) -8kV

Figure A.8: Ion Current Measurements - 35mm electrode spacing continued